arXiv:1704.00819v1 [hep-ph] 3 Apr 2017

Neutrino Mass, Leptogenesis and FIMP Dark Matter in a $U(1)_{B-L}$ Model

Anirban Biswas,[1,2,*] Sandhya Choubey,[1,2,3,†] and Sarif Khan[1,2,‡]

[1]*Harish-Chandra Research Institute, Chhatnag Road, Jhunsi, Allahabad 211 019, India*

[2]*Homi Bhabha National Institute, Training School Complex, Anushaktinagar, Mumbai - 400094, India*

[3]*Department of Theoretical Physics, School of Engineering Sciences, KTH Royal Institute of Technology, AlbaNova University Center, 106 91 Stockholm, Sweden*

Abstract

The Standard Model (SM) is unable to explain the origin of tiny neutrino masses, dark matter and matter-antimatter asymmetry of the Universe. In this work, we propose a model that can address all these three observations. Our model extends the SM by a local $U(1)_{B-L}$ gauge symmetry, three right-handed (RH) neutrinos to cancel the gauge anomalies, and two scalars, one of which is charged under $U(1)_{B-L}$ while the other is not. The $U(1)_{B-L}$ symmetry is broken spontaneously when the scalar charged under this gauge group picks up a VEV. This results in making both the additional neutral gauge boson as well as the RH neutrinos massive. The light neutrino masses can be generated easily in this model by the Type I seesaw mechanism. Here we consider phenomenologically interesting TeV scale RH Majorana neutrinos and two of them are nearly degenerate, which allows us to generate a lepton asymmetry via resonant leptogenesis. This lepton asymmetry is converted to the baryon asymmetry through sphaleron processes allowing us to correctly reproduce the observed matter-antimatter asymmetry of the Universe. Finally, the second new scalar which is neutral under the SM as well as $U(1)_{B-L}$ gauge group is made stable by adding a $\mathbb{Z}_2$ symmetry. We show that this particle can easily play the role of the dark matter of the Universe. Null results from direct detection experiments force us to think about the beyond thermal WIMP scenario. Thus, we consider our dark matter candidate to be very feebly interacting with the cosmic soup and hence it is called the FIMP which never attains thermal equilibrium. We study in detail the production of the dark matter via freeze-in mechanism before and after electroweak symmetry breaking and use the observed dark matter relic abundance to put constraints on relevant model parameters.

*Electronic address: anirbanbiswas@hri.res.in

†Electronic address: sandhya@hri.res.in

‡Electronic address: sarifkhan@hri.res.in

I. INTRODUCTION

The presence of non-zero neutrino mass and mixing has been confirmed by observing neutrino flavour oscillations [1, 2] among its different flavours. Neutrino experiments have measured the three intergenerational mixing angles $(\theta_{12}, \theta_{23}, \theta_{13})$ and the two mass square differences (Δm^2_{21} and Δm^2_{32}) [1] with an unprecedented accuracy [3–10]. Neutrinos are massless in the Standard Model (SM) of particle physics because in SM there is no right handed (RH) counterpart of the left handed (LH) neutrinos. To generate tiny neutrino masses and their intergenerational mixing angles, as suggested by different experiments, we have to think of some new interactions and/or new particles beyond the Standard Model (BSM). Moreover, there are still some unsolved problems in the neutrino sector. For example, we do not know the exact octant of the atmospheric mixing angle θ_{23} i.e. whether it lies in the lower octant ($\theta_{23} < 45^\circ$) or in the higher octant ($\theta_{23} > 45^\circ$), the exact sign of Δm^2_{32} which is related to the mass hierarchy between m_2 and m_3 (for the normal hierarchy (NH) $\Delta m^2_{32} > 0$ while for the inverted hierarchy (IH) $\Delta m^2_{32} < 0$) and also about the Dirac CP phase δ, responsible for the CP violation in the leptonic sector. Recently, T2K and NoνA experiments have reported their preliminary result which predicts that the value of Dirac CP phase is around $\delta_{CP} \sim 270^\circ$ [11]. Besides these, we do not know whether the neutrinos are Dirac fermion or Majorana fermion. Observation of neutrino less double β decay [12–17] will confirm the Majorana nature of neutrinos and might also provide important information about the Majorana phases which could be the other source of CP violation in the leptonic sector, if the SM neutrinos are Majorana fermions.

Besides these unsolved problems in the neutrino sector, another well known puzzle in recent times is the presence of dark matter (DM) in the Universe. Many indirect evidence suggests the existence of DM. Among the most compelling evidence of DM are the observed flatness of rotation curves of spiral galaxies [18], gravitational lensing [19, 20], the observed spatial offset between DM and visible matter in the collision of two galaxy clusters (e.g. Bullet cluster [23], Abel cluster [22]) etc. The latter also imposes an upper bound on the ratio between self interaction and mass of DM particles, which is $\frac{\sigma_{DM}}{M_{DM}} \lesssim 1\,\text{barn/GeV}$ [23]. Moreover, satellite borne experiments like WMAP [24] and Planck [25] have made a precise measurement of the amount of dark matter present in the Universe from the cosmic microwave background (CMB) anisotropy [25] and the current measured value of this parameter lies in the range $0.1172 \leq \Omega_{\rm DM} h^2 \leq 0.1226$ at 67% C.L [25].

Despite the compelling observational evidence for DM due to its gravitational interactions, our knowledge about its particle nature is very limited. The only thing we know about the DM is that it is very weakly interacting and electromagnetically blind. The SM of particle physics

[1] $\Delta m^2_{ij} = m^2_i - m^2_j$ and $\Delta m^2_{atm} = m^2_3 - \frac{m^2_1 + m^2_2}{2}$

does not have any fundamental particle which can play the role of a cold dark matter (CDM), consequently a BSM scenario containing new fundamental stable particle(s) is required. There are earth based ongoing DM direct detection experiments, namely Xenon-1T [26], LUX [27], CDMS [28] amongst others, which have been trying to detect the Weakly Interacting Massive Particle (WIMP) [29, 30] type DM by measuring recoil energies of the detector nuclei scattered by the WIMPs. However, no convincing DM signal has been found yet and hence the $M_{DM} - \sigma_{\rm SI}$ plane for a WIMP type DM is now getting severely constrained. Therefore, invoking particle DM models outside the WIMP paradigm seems to be pertinent at this stage. In the present work we study one of the possible alternatives of WIMP, namely, the Feebly Interacting Massive Particle (FIMP) [31–40]. A major difference between the WIMP and FIMP scenarios is that while in the former the DM particle is in thermal equilibrium with the plasma in the early Universe and freezes-out when the Hubble expansion rate becomes larger than its annihilation cross section, in the FIMP case the DM is never in thermal equilibrium with the cosmic soup. This is mainly ensured by its extremely weak couplings to other particles in the thermal bath. Therefore, the number density of the FIMP is negligible in the early Universe and increases when the FIMP is subsequently produced by the decays and annihilations of other particles to which it is coupled (very feebly). This process is generally known as freeze-in [31].

In addition to the above two unsolved problems, another long standing enigma is the presence of more baryons over anti baryons in the Universe, which is known as the baryon asymmetry or the matter-antimatter asymmetry in the Universe. The baryon asymmetry observed in the Universe is expressed by a quantity $Y_B = \dfrac{\eta_B\, n_\gamma}{\rm s}$, where $\eta_B = n_B - n_{\bar{B}}$ is the excess in the number density for baryon over anti-baryon while n_γ and s are the photon number density and the entropy density of the Universe, respectively. At the present epoch, $\eta_B = (5.8 - 6.6) \times 10^{-10}$ at 95% C.L. [41] while at $T \sim 2.73$ K, the photon density $n_\gamma = 410.7$ cm^{-3} [41] and the entropy density s $= 2891.2$ cm^{-3} [41] (in natural unit with Boltzmann constant $K_B = 1$). Therefore, the observed baryon asymmetry at the present Universe is $Y_B = (8.24 - 9.38) \times 10^{-10}$, which although small, is sufficient to produce the $\sim 5\%$ energy density (visible matter) of the Universe. To generate baryon asymmetry in the Universe from a matter-antimatter symmetric state, one has to satisfy three necessary conditions, known as the Sakharov's conditions [42]. These are i) baryon number (B) violation, ii) C and CP violation and iii) departure from thermal equilibrium. Since the baryon number (B) is an accidental symmetry of the SM (i.e. all SM interactions are B conserving) and also the observed CP violation in quark sector is too small to generate the requited baryon asymmetry, hence like the previous cases, here also one has to look for some additional BSM interactions which by satisfying the Sakharov's conditions can generate the observed baryon asymmetry in an initially matter-antimatter symmetric Universe.

In this work, we will try to address all of the three above mentioned issues. The non-observation of any BSM signal at LHC implies the concreteness of the SM. However to address

all the three problems, we need to extend the particles list and/or gauge group of SM because as already mentioned, SM is unable to explain either of them. In our model, we have extend the SM gauge group $\mathrm{SU(3)_c \times SU(2)_L \times U(1)_Y}$ by a local $\mathrm{U(1)_{B-L}}$ gauge group. Since we have imposed a local U(1) symmetry, consequently an extra gauge boson (Z_{BL}) will arise. To cancel the anomaly due to this extra gauge boson we need to introduce three right-handed (RH) neutrinos ($N_i, i = 1, 2, 3$) to make the model anomaly free. Apart from the three RH neutrinos, we have also introduced two SM gauge singlet scalars namely ϕ_H and ϕ_{DM}, where former is charged under the proposed $\mathrm{U(1)_{B-L}}$ group while latter has no $\mathrm{B-L}$ charge. The $\mathrm{U(1)_{B-L}}$ symmetry is spontaneously broken when the scalar field ϕ_H takes a nonzero vacuum expectation value (VEV) and thereby generates the masses for the three RH neutrinos as well as the extra neutral gauge boson Z_{BL}, whose mass terms are forbidden initially due to the $\mathrm{U(1)_{B-L}}$ invariance of the Lagrangian. The other scalar ϕ_{DM} does not take any VEV and we make it stable by imposing a $\mathbb{Z}_2$ parity. Hence, ϕ_{DM} can serve as a CDM candidate.

As mention above, the anomaly cancellation requires the introduction of three RH neutrinos in the model. Therefore we can easily generate the neutrino masses by the Type-I seesaw mechanism after B-L symmetry is broken. Diagonalising the light neutrino mass matrix (m_ν, for detail see Section III A), we determine the allowed parameter space by satisfying the 3σ bounds on the mass square differences (Δm^2_{12}, Δm^2_{atm}), the mixing angles ($\theta_{12}, \theta_{13}, \theta_{23}$) [57] and also the cosmological bound on the sum of three light neutrinos masses [25]. We also determine the effective mass $m_{\beta\beta}$ which is relevant for neutrino-less double beta decay and compare it against the current bound on $m_{\beta\beta}$ from GERDA phase I experiment [17].

Next, we explain the possible origin of the baryon asymmetry at the present epoch from an initially matter-antimatter symmetric Universe via leptogenesis. We first generate the lepton asymmetry (or $\mathrm{B-L}$ asymmetry, Y_{B-L}) from the out of equilibrium, CP violating decays of RH neutrinos. The lepton asymmetry thus produced has been converted to the baryon asymmetry by the $(B + L)$ violating sphaleron processes which are effective before and during electroweak phase transition [43–45]. When the sphaleron processes are in thermal equilibrium ($10^{12}\,\mathrm{GeV} \lesssim T \lesssim 10^2$ GeV, T being the temperature of the Universe), the conversion rate is given by [46]

$$Y_B = -\frac{8N_f + 4N_{\phi_h}}{22N_f + 13N_{\phi_h}} Y_{B-L} \tag{1}$$

where $N_f = 3$ and $N_{\phi_h} = 1$, are the number of fermionic generations and number of Higgs doublet in the model, respectively.

Finally, in order to address the dark matter issue, we consider the FIMP scenario. Here, scalar field ϕ_{DM} being a FIMP candidate, is mainly produced from the decays of heavy particles. In the non-thermal scenario, most of the production of the FIMP from the decay of a heavy particle occurs when $T \sim M$, where M is the mass of the decaying mother particle, which is in thermal equilibrium. Therefore, the non-thermality condition of the FIMP demands that

$\frac{\Gamma}{H} < 1\Big|_{T\sim M}$ [47], which in turn imposes a severe upper bound on the coupling strengths of the FIMP. Thus the non-thermality condition requires extremely small coupling of ϕ_{DM} with the thermal bath ($\lesssim 10^{-10}$) and hence, FIMP DM can easily evade all the existing bounds from DM direct detection experiments [26–28].

Rest of the paper has been arranged in the following manner, in Section II we discuss the model in detail. In Section III we present the main results of the paper. In particular, we discuss the neutrino phenomenology in Section III A, baryogenesis via leptogenesis in Section III B and non-thermal FIMP dark matter ϕ_{DM} production in Section III C. Finally in Section IV we end with our conclusions.

II. MODEL

The gauged $\mathrm{U(1)_{B-L}}$ extension of SM is one of the most extensively studied BSM model so far. In this model the gauge sector of the SM is enhanced by imposing a local $\mathrm{U(1)_{B-L}}$ symmetry to the SM Lagrangian, where B and L represent the respective baryon and lepton number of a particle. Therefore, the complete gauged group is $\mathrm{SU(3)_c \times SU(2)_L \times U(1)_Y \times U(1)_{B-L}}$. Since the $\mathrm{U(1)_{B-L}}$ extension of SM is not an anomaly free theory, hence we need to introduce some chiral fermions to cancel the anomaly. In order to achieve this, we have considered three extra right handed (RH) neutrinos to make the proposed $\mathrm{B-L}$ extension anomaly free. Besides the SM particles and three RH neutrinos, we have introduced a SM gauge singlet scalar ϕ_H in the theory with a suitable $\mathrm{B-L}$ charge, which breaks the proposed $\mathrm{U(1)_{B-L}}$ symmetry spontaneously by acquiring a nonzero VEV v_{BL} and thereby generates masses for all the BSM particles. Furthermore, we have also added another real scalar field ϕ_{DM} which is singlet under the aforementioned gauge group but possesses an odd $\mathbb{Z}_2$ charge, while all the other particles in the model (both SM and BSM) are even under the considered $\mathbb{Z}_2$ parity. Hence, the Lagrangian of our model does not contain any interaction term involving odd powers of ϕ_{DM}. The $\mathbb{Z}_2$ invariance of the Lagrangian will be preserved if the parameters of the Lagrangian are such that the scalar field ϕ_{DM} does not get any VEV. For this case, the real scalar field ϕ_{DM} becomes absolutely stable and, in principle, can serve as a viable dark matter candidate. The respective $\mathrm{SU(2)_L}$, $\mathrm{U(1)_Y}$, $\mathrm{U(1)_{B-L}}$ and $\mathbb{Z}_2$ charges of all the particles in the present model are listed in Table I.

Gauge	Baryon Fields			Lepton Fields			Scalar Fields		
Group	$Q_L^i=(u_L^i,d_L^i)^T$	u_R^i	d_R^i	$L_L^i=(\nu_L^i,e_L^i)^T$	e_R^i	N_R^i	ϕ_h	ϕ_H	ϕ_{DM}
$\mathrm{SU(2)_L}$	2	1	1	2	1	1	2	1	1
$\mathrm{U(1)_Y}$	1/6	2/3	−1/3	−1/2	−1	0	1/2	0	0
$\mathrm{U(1)_{B-L}}$	1/3	1/3	1/3	−1	−1	−1	0	2	0
$\mathbb{Z}_2$	+	+	+	+	+	+	+	+	−

Table I: Charges of all particles under various symmetry groups.

The complete Lagrangian for the model is as follows,

$$\begin{aligned}\mathcal{L} \;=\; & \mathcal{L}_{SM}+\mathcal{L}_{DM}+(D_\mu\phi_H)^\dagger(D^\mu\phi_H)-\frac{1}{4}F_{BL\mu\nu}F_{BL}{}^{\mu\nu}+\frac{i}{2}\bar{N}_i\gamma^\mu D_\mu N_i-V(\phi_h,\phi_H)\\ & -\sum_{i=1}^{3}\frac{y_{N_i}}{2}\phi_H\bar{N}_i^c N_i-\sum_{i,\,j=1}^{3}y'_{ij}\bar{L}_i\tilde{\phi}_h N_j+h.c.\,,\end{aligned} \tag{2}$$

with $\tilde{\phi_h}=i\sigma_2\phi_h^*$. The term $\mathcal{L}_{SM}$ and $\mathcal{L}_{DM}$ represent the SM and dark sector Lagrangian, respectively. The dark sector Lagrangian $\mathcal{L}_{DM}$ containing all possible gauge invariant interaction terms of a real scalar field ϕ_{DM}, has the following form

$$\begin{aligned}\mathcal{L}_{DM} \;=\; & \frac{1}{2}(\partial^\mu\phi_{DM})(\partial_\mu\phi_{DM})-\frac{\mu_{DM}^2}{2}\phi_{DM}^2-\lambda_{DM}\,\phi_{DM}^4-\lambda_{Dh}\,\phi_{DM}^2(\phi_h^\dagger\phi_h)\\ & -\lambda_{DH}\,\phi_{DM}^2(\phi_H^\dagger\phi_H)\,,\end{aligned} \tag{3}$$

where the interactions of ϕ_{DM} with ϕ_h and ϕ_H are proportional to the couplings λ_{Dh} and λ_{DH}, respectively. The fourth term in Eq. (2) represents the kinetic term for the additional gauge boson Z_{BL}^μ in terms of field strength tensor $F_{BL\mu\nu}$ of the $\mathrm{U(1)_{B-L}}$ gauge group. The covariant derivatives involved in the kinetic energy terms of ϕ_H and N_i in Eq. (2), can be expressed by the following generic form

$$D_\mu\psi=(\partial_\mu+i\,g_{BL}\,Q_{BL}(\psi)\,Z_{BL\mu})\,\psi\,, \tag{4}$$

where $\psi=\phi_H$, N_i and $Q_{BL}(\psi)$ represents the $\mathrm{U(1)_{B-L}}$ charge of the corresponding field (listed in Table I). The quantity $V(\phi_h,\phi_H)$ in Eq. (2) contains the self interaction terms of ϕ_H and ϕ_h as well as the mutual interaction term between the two scalar fields. The expression of $V(\phi_h,\phi_H)$ is given by

$$V(\phi_h,\phi_H)=\mu_H^2\phi_H^\dagger\phi_H+\mu_h^2\phi_h^\dagger\phi_h+\lambda_H(\phi_H^\dagger\phi_H)^2+\lambda_h(\phi_h^\dagger\phi_h)^2+\lambda_{hH}(\phi_h^\dagger\phi_h)(\phi_H^\dagger\phi_H)\,. \tag{5}$$

After the symmetry breaking, the SM Higgs doublet ϕ_h and the BSM scalar ϕ_H take the following form,

$$\phi_h = \begin{pmatrix} 0 \\ \dfrac{v+H}{\sqrt{2}} \end{pmatrix} \qquad \phi_H = \left(\frac{v_{BL} + H_{BL}}{\sqrt{2}} \right) \,, \tag{6}$$

where $v = 246$ GeV is the VEV of ϕ_h, which breaks the SM gauge symmetry into a residual $\mathrm{U(1)_{EM}}$ symmetry. The remaining terms in Eq. (2) are the Yukawa interaction terms for the left handed and right handed neutrinos. As mentioned in the beginning of this section, when the extra scalar field ϕ_H gets a nonzero VEV v_{BL}, the proposed $\mathrm{U(1)_{B-L}}$ gauge symmetry breaks spontaneously. As a results, the Majorana mass terms for the right handed neutrinos, proportional to the Yukawa couplings Y_{N_i}, are generated. In general, for a three generation of right handed neutrinos, we will have a 3×3 Majorana mass matrix $\mathcal{M}_{\mathcal{R}}$ with all off diagonal terms are present. However, in the present scenario for calculational simplicity, we have chosen a basis for the N_i fields with respect to which $\mathcal{M}_{\mathcal{R}}$ is diagonal. The diagonal elements, representing the masses of N_is, are given by,

$$M_{N_i} \;=\; \frac{y_{N_i}}{\sqrt{2}} v_{BL} \,. \tag{7}$$

Like the three right handed neutrinos, the extra neutral gauge bosons also becomes massive through the Eq. (4) when ϕ_H picks up a VEV. The mass term Z_{BL} is given by

$$M_{Z_{BL}} \;=\; 2\, g_{BL}\, v_{BL} \,. \tag{8}$$

When both ϕ_h and ϕ_H obtain their respective VEVs, there will be a mass mixing between the states H and H_{BL}. The mass matrix with respect to the basis H and H_{BL} looks like as follows

$$\mathcal{M}^2_{scalar} = \begin{pmatrix} 2\lambda_h v^2 & \lambda_{hH}\, v_{BL}\, v \\ \\ \lambda_{hH}\, v_{BL}\, v & 2\lambda_H v_{BL}^2 \end{pmatrix} \,. \tag{9}$$

Rotating the basis states H and H_{BL} by a suitable angle α, we can make the above mass matrix diagonal. The new basis states (h_1 and h_2) with respect to which the mass matrix $\mathcal{M}^2_{scalar}$ becomes diagonal, are some linear combinations of earlier basis states H and H_{BL}. The new basis states, now representing two the physical states, are defined as

$$\begin{aligned} h_1 \;&=\; H \cos\alpha + H_{BL} \sin\alpha \,, \\ h_2 \;&=\; -H \sin\alpha + H_{BL} \cos\alpha \,, \end{aligned} \tag{10}$$

where we denote h_1 as the SM-like Higgs boson while h_2 is playing the role of a BSM scalar field. The mixing angle between H and H_{BL} can be expressed in terms of the parameters of the

Lagrangian (cf. Eq. (2)) as,

$$\tan 2\alpha = \frac{\lambda_{hH}\, v_{BL}\, v}{\lambda_h v^2 - \lambda_H v_{BL}^2}\,. \tag{11}$$

Besides the two physical scalar fields h_1 and h_2, as mentioned earlier, there is another real scalar field (ϕ_{DM}) in the present model, which can play the role of a dark matter candidate. The masses of these three physical scalar fields h_1, h_2 and ϕ_{DM} are give below,

$$\begin{aligned}
M_{h_1}^2 &= \lambda_h v^2 + \lambda_H v_{BL}^2 - \sqrt{(\lambda_h v^2 - \lambda_H v_{BL}^2)^2 + (\lambda_{hH}\, v\, v_{BL})^2}\,, \\
M_{h_2}^2 &= \lambda_h v^2 + \lambda_H v_s^2 + \sqrt{(\lambda_h v^2 - \lambda_H v_{BL}^2)^2 + (\lambda_{hH}\, v\, v_{BL})^2}\,, \\
M_{DM}^2 &= \mu_{DM}^2 + \lambda_{Dh} v^2 + \lambda_{DH} v_{BL}^2\,,
\end{aligned} \tag{12}$$

where ${M_x}^2$ denotes the mass of the corresponding scalar field x.

In this work, we choose M_{h_2}, M_{DM}, M_{N_i}, $M_{Z_{BL}}$, g_{BL}, α, λ_{Dh}, λ_{DH} and λ_{DM} as our independent set of parameters. The other parameters in the Lagrangian namely λ_h, λ_H, λ_{hH}, $\mu_{\phi_h}^2$ and $\mu_{\phi_H}^2$ can be expressed in terms of these variables as follows [54].

$$\begin{aligned}
\lambda_H &= \frac{M_{h_1}^2 + M_{h_2}^2 + (M_{h_2}^2 - M_{h_1}^2)\cos 2\alpha}{4\, v_{BL}^2}\,, \\
\lambda_h &= \frac{M_{h_1}^2 + M_{h_2}^2 + (M_{h_1}^2 - M_{h_2}^2)\cos 2\alpha}{4\, v^2}\,, \\
\lambda_{hH} &= \frac{(M_{h1}^2 - M_{h_2}^2)\cos\alpha \sin\alpha}{v\, v_{BL}}\,, \\
\mu_{\phi_h}^2 &= -\frac{(M_{h_1}^2 + M_{h_2}^2)v + (M_{h_1}^2 - M_{h_2}^2)(v\cos 2\alpha + v_{BL}\sin 2\alpha)}{4\, v}\,, \\
\mu_{\phi_H}^2 &= \frac{-(M_{h_1}^2 + M_{h_2}^2)v_{BL} + (M_{h_1}^2 - M_{h_2}^2)(v_{BL}\cos 2\alpha - v\sin 2\alpha)}{4\, v_{BL}}\,, \\
\mu_{DM}^2 &= M_{DM}^2 - \lambda_{Dh} v^2 - \lambda_{DH} v_{BL}^2\,,
\end{aligned} \tag{13}$$

where v_{BL} is defined in terms of $M_{Z_{BL}}$ and g_{BL} in Eq. (8).

In the present scenario, two of the three scalar fields namely ϕ_h and ϕ_H obtain VEVs. On the other hand, the remaining scalar field ϕ_{DM} does not have any VEV, which ensures its stability by preserving its $\mathbb{Z}_2$ odd parity. Therefore, the ground state of the system is ($\langle\phi_h\rangle$, $\langle\phi_H\rangle$, $\langle\phi_{DM}\rangle$) = (v, v_{BL}, 0). Now, such a ground state (vacuum) will be bounded from below when the following

[2] Throughout the paper we have kept the mass (M_{h_1}) of SM-like Higgs boson h_1 fixed at 125.5 GeV.

inequalities are satisfied simultaneously [54],

$$
\begin{aligned}
&\mu_{\phi_h}^2 < 0, \mu_{\phi_H}^2 < 0, \mu_{DM}^2 > 0\,, \\
&\lambda_h \geq 0, \lambda_H \geq 0, \lambda_{DM} \geq 0, \\
&\lambda_{hH} \geq -2\sqrt{\lambda_h\,\lambda_H}, \\
&\lambda_{Dh} \geq -2\sqrt{\lambda_h\,\lambda_{DM}}, \\
&\lambda_{DH} \geq -2\sqrt{\lambda_H\,\lambda_{DM}}, \\
&\sqrt{\lambda_{hH} + 2\sqrt{\lambda_h\,\lambda_H}}\sqrt{\lambda_{Dh} + 2\sqrt{\lambda_h\,\lambda_{DM}}}\sqrt{\lambda_{DH} + 2\sqrt{\lambda_H\,\lambda_{DM}}} \\
&+2\,\sqrt{\lambda_h\lambda_H\lambda_{DM}} + \lambda_{hH}\sqrt{\lambda_{DM}} + \lambda_{Dh}\sqrt{\lambda_H} + \lambda_{DH}\sqrt{\lambda_h} \geq 0 \quad . \qquad (14)
\end{aligned}
$$

Besides the lower limits as described by the above inequalities, there are also upper limits on the Yukawa and quartic couplings arising from the perturbativity condition which demands that the Yukawa and scalar quartic couplings have to be less than $\sqrt{4\,\pi}$ ($y < \sqrt{4\,\pi}$) and $4\,\pi$ ($\lambda < 4\,\pi$) respectively [55].

III. RESULTS

A. Neutrino Masses and Mixing

As mentioned earlier, the cancellation of both axial vector anomaly [58, 59] and gravitational gauge anomaly [60, 61], in $\mathrm{U(1)_{B-L}}$ extended SM, requires the presence of extra chiral fermions. Hence, in the present model to cancel these anomalies we have introduced three right handed (RH) neutrinos (N_i, i=1 to 3). The Majorana masses for the RH neutrinos are generated only after spontaneous breaking of the proposed $\mathrm{B-L}$ symmetry by the VEV of ϕ_H. Also in the present scenario, as stated earlier, we are working in a basis where the Majorana mass matrix for the three RH neutrinos are diagonal i.e. $\mathcal{M}_{\mathcal{R}} = \mathrm{diag}\,(M_{N_1}, M_{N_2}, M_{N_3})$. The expression for the mass of ith RH neutrino (M_{N_i}) is given in Eq. (7). On the other hand, the Dirac mass terms involving both left chiral and right chiral neutrinos, are originated when the electroweak symmetry is spontaneously broken by the VEV of SM Higgs doublet ϕ_h, giving rise to a 3×3 complex hermitian matrix $\mathcal{M}_{\mathcal{D}}$. In general, one can take all the elements of matrix $\mathcal{M}_{\mathcal{D}}$ as complex but for simplicity and also keeping in mind that only three physical phases (one Dirac phase and two Majorana phases) exist for three light neutrinos (Majorana type), we have considered only three complex elements in the lower triangle part of the Dirac mass matrix $\mathcal{M}_{\mathcal{D}}$.

Hence for the Dirac mass matrix $\mathcal{M}_{\mathcal{D}}$ we assume the following structure:

$$\mathcal{M}_D = \begin{pmatrix} y_{ee} & y_{e\mu} & y_{e\tau} \\ y_{\mu e} + i\,\tilde{y}_{\mu e} & y_{\mu\mu} & y_{\mu\tau} \\ y_{\tau e} + i\,\tilde{y}_{\tau e} & y_{\tau\mu} + i\,\tilde{y}_{\tau\mu} & y_{\tau\tau} \end{pmatrix} , \tag{15}$$

where $y_{ij} = \dfrac{y'_{ij}}{\sqrt{2}} v$ $(i, j = \mathrm{e}, \mu, \tau)$ and the Yukawa coupling y'_{ij} has been defined in Eq. (2).

Now, with respect to the Majorana basis $\left(\overline{\nu_{\alpha L}} \;\; \overline{(N_{\alpha R})^c}\right)^T$ and $\left((\nu_{\alpha L})^c \;\; N_{\alpha R}\right)^T$ one can write down the Majorana mass matrix for both left and right chiral neutrinos using $\mathcal{M}_{\mathcal{D}}$ and $\mathcal{M}_{\mathcal{R}}$ matrices in the following way,

$$M = \begin{pmatrix} 0 & \mathcal{M}_{\mathcal{D}} \\ \mathcal{M}_{\mathcal{D}}{}^T & \mathcal{M}_{\mathcal{R}} \end{pmatrix} . \tag{16}$$

Since M_D and M_R are both 3×3 matrices (for three generations of neutrinos), the resultant matrix M will be of order 6×6 and also it is a complex symmetric matrix which reflects its Majorana nature. Therefore, after diagonalisation of the matrix M, we get three light and three heavy neutrinos, all of which are Majorana fermions. If we use the block diagonalisation technique, we can write the light and heavy neutrino mass matrices in the leading order as,

$$m_\nu \;\simeq\; -\mathcal{M}_{\mathcal{D}}\, \mathcal{M}_{\mathcal{R}}{}^{-1} \mathcal{M}_{\mathcal{D}}{}^T , \tag{17}$$

$$m_N \;\simeq\; \mathcal{M}_{\mathcal{R}} . \tag{18}$$

Here M_R is a diagonal matrix while for the diagonalisation of the complex symmetric matrix m_ν, we have introduced a Hermitian matrix h which is $h = m_\nu m_\nu^\dagger$. The expression of all the elements of m_ν in terms of the elements of $\mathcal{M}_{\mathcal{D}}$ and $\mathcal{M}_{\mathcal{R}}$ matrices are given in Appendix A. We can diagonalise the Hermitian matrix h by a similarity transformation using a Unitary matrix U_{PMNS},

$$U_{\mathrm{PMNS}}^\dagger\, h\, U_{\mathrm{PMNS}} = \mathrm{diag}\,(m_1^2, m_2^2, m_3^2) = h_D \tag{19}$$

and the Unitary matrix U_{PMNS} is parametrised in the following form,

$$U_{\mathrm{PMNS}} = \begin{pmatrix} c_{12}c_{13} & e^{i\frac{\alpha}{2}} s_{12}c_{13} & s_{13}e^{-i(\delta - \frac{\beta}{2})} \\ -s_{12}c_{23} - c_{12}s_{23}s_{13}e^{i\delta} & e^{i\frac{\alpha}{2}}(c_{12}c_{23} - s_{12}s_{13}s_{23}e^{i\delta}) & c_{13}s_{23}e^{i\frac{\beta}{2}} \\ s_{12}s_{23} - c_{12}s_{13}c_{23}e^{i\delta} & e^{i\frac{\alpha}{2}}(-c_{12}s_{23} - s_{12}s_{13}c_{23}e^{i\delta}) & c_{13}c_{23}e^{i\frac{\beta}{2}} \end{pmatrix} , \tag{20}$$

where $c_{ij} = \cos\theta_{ij}$, $s_{ij} = \sin\theta_{ij}$ and $\theta_{ij} \in [0, \frac{\pi}{2}]$. Here θ_{ij} represents the light neutrino mixing angles between ith and jth generations while δ and α, β are Dirac CP phase and two Majorana

phases respectively with $\alpha, \beta, \delta \in [0, 2\pi]$. After diagonalising the h matrix using Eqs. (19) and (20), we can easily determine the three mixing angles θ_{12}, θ_{23} and θ_{13} and three mass eigenvalues. To determine the Dirac CP phase δ, we have used the Jarlskog Invariant $J_{\rm CP}$ [56] which is defined as,

$$J_{\rm CP} = \frac{1}{8} \sin 2\theta_{12} \sin 2\theta_{23} \sin 2\theta_{13} \cos\theta_{13} \sin\delta. \tag{21}$$

The quantity $J_{\rm CP}$ is related to the elements of the matrix h in the following way,

$$J_{CP} = \frac{{\rm Im}\,(h_{13} h_{23} h_{31})}{\Delta m^2_{21}\,\Delta m^2_{32}\,\Delta m^2_{31}} \tag{22}$$

where in the numerator ${\rm Im}(X)$ represents the imaginary part of X while in the denominator, $\Delta m^2_{ij} = m^2_i - m^2_j$. Once we determine the quantity $J_{\rm CP}$ (from Eq. (22)) and the intergenerational mixing angles of neutrinos then one can easily determine the Dirac CP phase using Eq. (21).

In the present scenario we have twelve independent parameters coming from the Dirac mass matrix. The RH neutrino mass matrix, in principle, should bring in three additional parameters. However, as we will discuss in details in Section III B, two of the RH neutrino masses is taken to be nearly degenerate. In particular, the condition of resonant leptogenesis requires that $M_{N_2} - M_{N_1} = \Gamma_1/2$, where Γ_1 is the tree level decay width of N_1 and is seen to be $\sim 10^{-11}$ GeV. Therefore, for all practical purposes we have $M_{N_1} \simeq M_{N_2}$, and the RH neutrino mass matrix only brings in two independent parameters, M_{N_1} and M_{N_3}. Thus, we have fourteen independent parameters which we vary in the following ranges,

$$\begin{aligned}
1\ {\rm TeV} \;&\leq\; M_{N_1} \;&&\leq\; 3\ {\rm TeV}\,, \\
M_{N_1} \;&<\; M_{N_3} \;&&\leq\; 15\ {\rm TeV}\,, \\
1 \;&\leq\; \frac{\sqrt{2}\ y_{ij}}{v} \times 10^8 \;&&\leq\; 1000 \qquad (i, j = e,\ \mu,\ \tau, i = j \neq e)\,, \\
1 \;&\leq\; \frac{\sqrt{2}\ y_{ee}}{v} \times 10^{10} \;&&\leq\; 100\,, \\
1 \;&\leq\; \frac{\sqrt{2}\ \tilde{y}_{ij}}{v} \times 10^8 \;&&\leq\; 1000 \qquad (i = \tau, j = e,\ \mu)\,, \\
1 \;&\leq\; \frac{\sqrt{2}\ \tilde{y}_{\mu e}}{v} \times 10^9 \;&&\leq\; 1000\,.
\end{aligned} \tag{23}$$

We try to find the allowed parameter space which satisfy the following constraints on three mixing angles (θ_{ij}) and two mass square differences (Δm^2_{ij}), J_{CP} obtained from neutrino oscillation data and the cosmological bound on the sum of three light neutrino masses. These experimental/observational results are listed below.

- Measured values of three mixing angles in 3σ range [57]:
  $30^\circ < \theta_{12} < 36.51^\circ$, $37.99^\circ < \theta_{23} < 51.71^\circ$ and $7.82^\circ < \theta_{13} < 9.02^\circ$.

- Allowed values of two mass squared differences in 3σ range [57]:
  $6.93 < \dfrac{\Delta m^2_{21}}{10^{-5}}\,\text{eV}^2 < 7.97$ and $2.37 < \dfrac{\Delta m^2_{31}}{10^{-3}}\,\text{eV}^2 < 2.63$ in 3σ range.
- Above mentioned values of the neutrino oscillation parameters also put an upper bound on the absolute value of $J_{\rm CP}$ from Eq. (21), which is $|J_{\rm CP}| \leq 0.039$.
- Cosmological upper bound on the sum of three light neutrino masses i.e. $\sum_i m_i < 0.23$ eV at 2σ C.L. [25].

While it is possible to obtain both normal hierarchy (NH) ($m_1 < m_2 < m_3$) and inverted hierarchy (IH) ($m_3 < m_1 < m_2$) in this scenario, we show our results only for NH for brevity. Similar results can be obtained for IH.

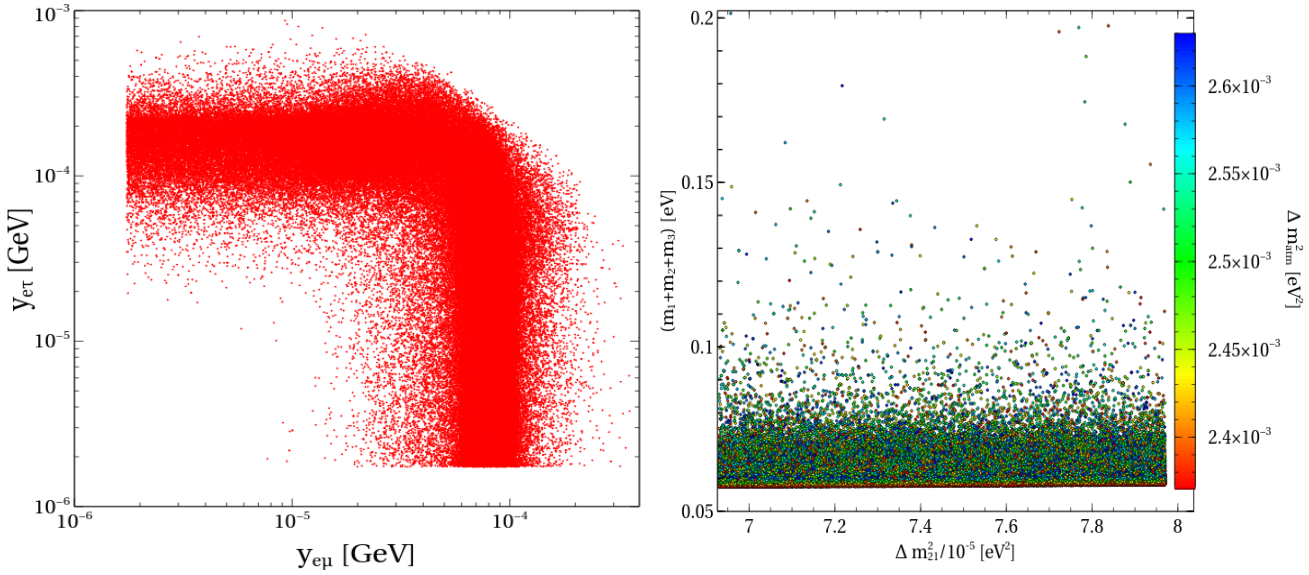

Figure 1: **Left panel:** Allowed region in $y_{e\mu} - y_{e\tau}$ plane. **Right panel:** Variation of sum of all three light neutrino masses with two mass square differences.

In the left panel (LP) of Fig. 1, we have shown the allowed parameter space in the $y_{e\mu} - y_{e\tau}$ plane which satisfies the neutrino oscillation parameters in its current 3σ range. While plotting this figure other relevant parameters have been scanned over their entire considered ranges mentioned in Eq. (23). From this plot, one can see that the neutrino oscillation data is satisfied only when the value of one parameter say $y_{e\mu}$ is small ($< 10^{-4}$) the other parameter $y_{e\tau}$ is large ($\gtrsim 10^{-4}$) or vice versa. They both can not be small ($\lesssim 10^{-5}$) simultaneously. On the other hand, in the right panel (RP) we have shown the variation of sum of three light neutrino masses ($\sum_i m_{\nu_i}$) with mass square difference Δm^2_{21} while the range of values of $\Delta m^2_{\rm atm} = m_3^2 - \dfrac{m_2^2 + m_1^2}{2}$ have been indicated by the colour bar. From this plot it is seen that in the present scenario, although the

full 3σ range Δm^2_{21} is satisfied, however the allowed values of $\sum_i m_{\nu_i}$ are mainly concentrated around $\sim 0.06 - 0.09$ eV. From colour bar one can easily identify that the corresponding values of $\Delta m^2_{\rm atm}$ are mostly concentrated around $\sim 2.45 \times 10^{-3}$ eV^2 to 2.55^{-3} eV^2 (green band in colour bar).

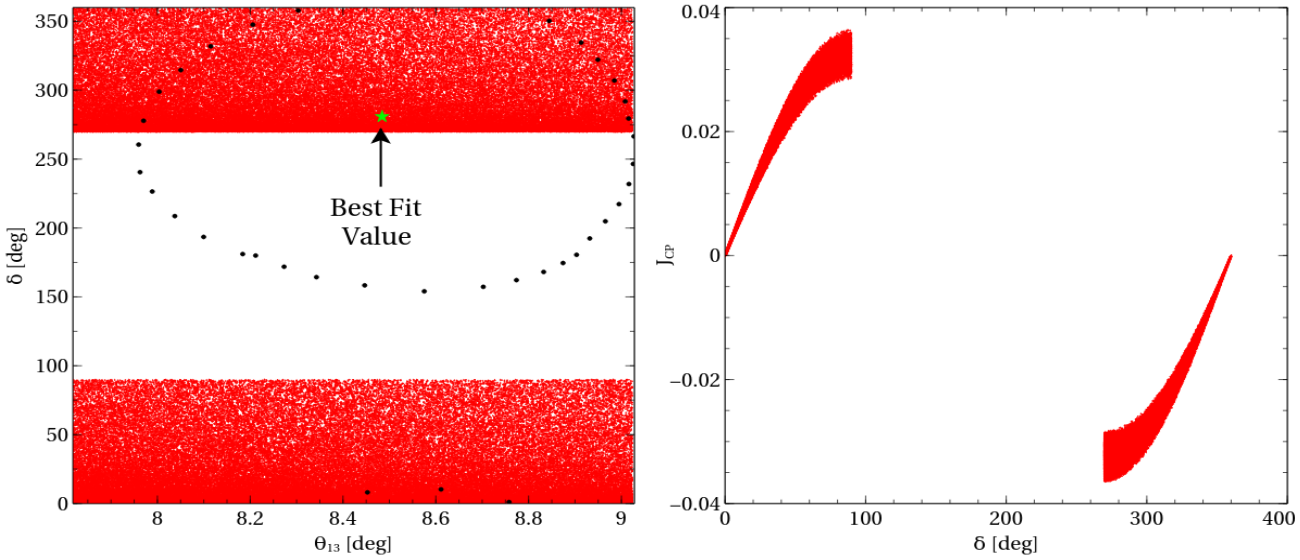

Figure 2: **LP:** Variation of Dirac CP phase δ with reactor mixing angle θ_{13}. Best fit value of δ as reported by T2K experiment has been indicated by a green coloured star. **RP:** Variation of $J_{\rm cp}$ with δ.

In the LP of Fig. 2, we have shown the variation of Dirac CP phase δ with the reactor mixing angle θ_{13}. From this plot one can see that there are two allowed ranges of Dirac CP phase $0^\circ \leq \delta \leq 90^\circ$ and $270^\circ \leq \delta \leq 360^\circ$ respectively which can reproduce the neutrino oscillation parameters in 3σ range. Recently T2K experiment has reported a preliminary result on δ to be around 270° [11] and that result is shown by a green coloured star in the LP of Fig. 2. The black dots represent the 3σ range of allowed δ with the reactor mixing angle θ_{13}. Therefore, although the present scenario predicts two ranges of δ, one in the entire first quadrant and another one is the entire fourth quadrant, however in the light of resent T2K results the latter one is more favourable. In the RP of Fig. 2, we have shown the variation of $J_{\rm CP}$ parameter (as defined in Eq. (21)) with the Dirac CP phase δ. Since the Jarlskog invariant $J_{\rm CP}$ is proportional to $\sin\delta$ and and since from the LP of Fig. 2, we see that δ can vary either between $0^\circ - 90^\circ$ or between $270^\circ - 360^\circ$, hence we get both positive and negative values of J_{CP} symmetrically placed in the first and fourth quadrants. However, the absolute values of $J_{\rm CP}$ always lie below 0.039.

In the LP of Fig. 3, we have plotted the variation of m_2 with m_1 (red coloured line) and m_3 with m_1 (greed coloured line). Since we are considering the normal hierarchical case, hence m_3 is always larger than m_2 and m_1. From this figure, we see that initially for smaller values of

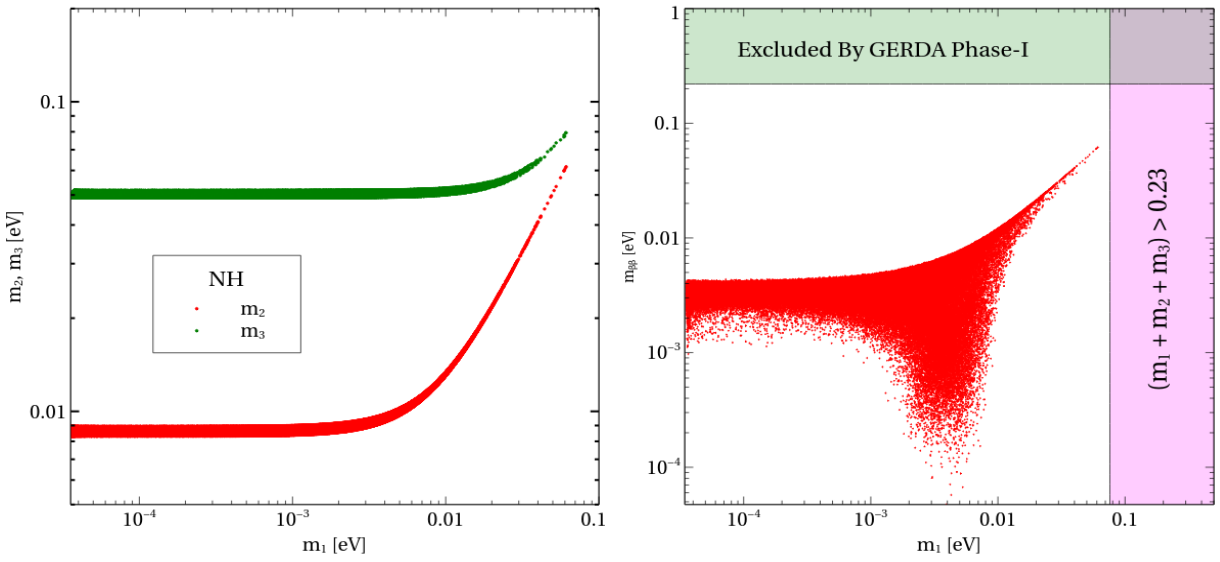

Figure 3: **LP:** Variation of m_2 and m_3 with the mass of lightest active neutrino m_1. **RP:** Variation of neutrino less double β decay parameter $m_{\beta\beta}$ with m_1.

m_1, m_2 remains almost horizontal and after a certain value of $m_1 \sim 0.01$ eV, m_2 rises rapidly. The sharp increase of m_2 for the relatively larger values of m_1 ($m_1 \gtrsim 0.01$ eV) is to keep the mass squared difference Δm^2_{21} within the experimentally allowed range. For the same reason, in order to remain within the experimentally predicted ranges of Δm^2_{31}, m_3 also increases with large values of m_1. However, in our case since $m_3 >> m_1$, hence this increment of m_3 with respect to m_1 is not as sharp as that of m_2 with m_1. In the RP of Fig. 3, we have shown the variation of neutrino less double β decay parameter $m_{\beta\beta}$ with the mass of lightest neutrino m_1. $m_{\beta\beta}$ is an important quantity for the study of neutrino less double β decay as the cross section of this process is proportional to $m_{\beta\beta} = \left|\sum_{i=1}^{3} (U_{\rm PMNS})^2_{ei}\, m_i\right| = (m_\nu)_{ee}$ (see Appendix B for details.), where $(m_\nu)_{ee}$ (Eq. A1) is the (1,1) element of light neutrino mass matrix m_ν. The nature of this plot is very to similar to the usual plot in $m_{\beta\beta} - m_1$ plane for the normal hierarchical scenario [62]. In the same plot, we have also shown the current bound on $m_{\beta\beta}$ from GERDA phase-I experiment [17].

B. Baryogenesis via Resonant Leptogenesis

Since we have three RH neutrinos, in this section we have studied the lepton asymmetry generated from the out of equilibrium decays of these heavy neutrinos at the early stage of the Universe. The B − L asymmetry thus produced is converted into the baryon asymmetry through sphaleron transitions which violate B + L quantum number while conserving the B − L charge.

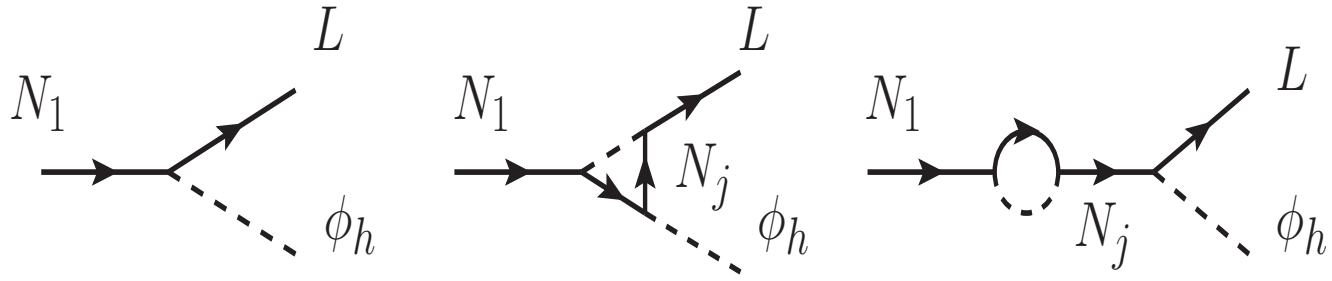

Figure 4: Feynmann diagrams for the decay of lightest RH neutrino N_1.

The sphaleron processes are active between temperatures of $\sim 10^{12}$ GeV to $\sim 10^2$ GeV in the early Universe. At high temperatures the sphalerons are in thermal equilibrium and subsequently they freeze-out at around $T \simeq 100 - 200$ GeV [50], just before electroweak symmetry breaking (EWSB). To produce sufficient lepton asymmetry, which would eventually be converted into the observed baryon asymmetry, one requires RH neutrinos with masses $\gtrsim 10^8 - 10^9$ GeV [48, 49]. This is the well know scenario of the "normal" or "canonical" leptogenesis. However, detection of these very massive RH neutrinos is beyond the reach of LHC and other future colliders. Here we consider the RH neutrinos to be in TeV mass range to allow for their detection at collider experiments. It has been shown that with RH neutrinos in the TeV mass-scale range, it is possible to generate adequate lepton asymmetry by considering the two lightest RH neutrinos N_1 and N_2 to be almost degenerate. More specifically, we demand that $M_{N_2} - M_{N_1} \simeq \Gamma_1/2$, where Γ_1 [3] is the total decay width of the lightest RH neutrino N_1. This scenario is known as Resonant leptogenesis [50, 52, 53].

Fig. 4 shows the tree level as well as one loop decay diagrams of the lightest RH neutrino N_1. These diagrams are applicable for all the three RH neutrinos. Here L represents the SM lepton which can either be a charged lepton or a left chiral neutrino depending on the nature of the scalar field (charged [4] or neutral) associated in the vertex while N_j denotes the remaining two RH neutrinos, N_2 and N_3 for the case of N_1 decay. In order to produce baryon asymmetry in the Universe we need both C and CP violating interactions, which is one of the three necessary conditions (see Sakharov conditions [42] given in Section I) for baryogenesis. The amount of lepton asymmetry generated in the out of equilibrium decay of the RH neutrino N_i is parametrised

[3] The typical value of Γ_1 is $\sim 10^{-11}$ GeV (see Fig. 5) while $M_{N_i} \sim \mathcal{O}(\text{TeV})$. Hence we take $M_{N_1} = M_{N_2}$ throughout the work.

[4] Since these processes occurred before EWSB hence we have both charged as well as neutral scalars in the SM.

by the CP asymmetry parameter (ε_i), which is defined as,

$$\varepsilon_i = \frac{\sum_j \left[\Gamma(N_i \to L_j\,\phi_h) - \Gamma(N_i \to \bar{L}_j\,\phi_h{}^\star)\right]}{\sum_j \left[\Gamma(N_i \to L_j\,\phi_h) + \Gamma(N_i \to \bar{L}_j\,\phi_h{}^\star)\right]}\,. \tag{24}$$

If we consider only the tree level decay process of N_i (first diagram in Fig. 4), there will not be any CP violation. The nonzero CP asymmetry is generated only by the interference between the tree level and the one loop level diagrams. The expression of CP asymmetry parameter (ε_i) is given by [51–53],

$$\varepsilon_i = -\sum_{j\neq i} \frac{M_{N_i}}{M_{N_j}} \frac{\Gamma_j}{M_{N_j}} \left(\frac{V_j}{2} + S_j\right) \frac{\mathrm{Im}\left[(\mathcal{M}_{\mathcal{D}}\mathcal{M}_{\mathcal{D}}{}^\dagger)^2_{ij}\right]}{(\mathcal{M}_{\mathcal{D}}\mathcal{M}_{\mathcal{D}}{}^\dagger)_{ii}\,(\mathcal{M}_{\mathcal{D}}\mathcal{M}_{\mathcal{D}}{}^\dagger)_{jj}}, \tag{25}$$

where V_j and S_j are the contributions coming from the vertex correction and the self energy correction diagrams respectively (second and third diagrams in Fig. 4). The expressions of V_j and S_j have the following forms [51–53],

$$\begin{aligned} V_j &= 2\frac{M^2_{N_j}}{M^2_{N_i}}\left[\left(1+\frac{M^2_{N_j}}{M^2_{N_i}}\right)\log\left(1+\frac{M^2_{N_i}}{M^2_{N_j}}\right) - 1\right], \\ S_j &= \frac{M^2_{N_j}\Delta M^2_{ij}}{(\Delta M^2_{ij})^2 + M^2_{N_i}\Gamma^2_j}\,, \end{aligned} \tag{26}$$

with

$$\Delta M^2_{ij} = M^2_{N_j} - M^2_{N_i}, \tag{27}$$

and Γ_j denotes the tree level decay width of the RH neutrino N_j (neglecting subdominant one loop corrections), which is given by [5]

$$\Gamma_j = \frac{M_{N_j}}{4\pi v^2}(\mathcal{M}_{\mathcal{D}}\mathcal{M}_{\mathcal{D}}{}^\dagger)_{jj}\ . \tag{28}$$

Now, as mentioned in the beginning of this section, the enhancement in the CP asymmetry factor (Eq. (24)) occurs when two RH neutrinos are almost degenerate i.e. $M_{N_2} - M_{N_1} \simeq \dfrac{\Gamma_1}{2}$. This is know as the resonance condition. In the present scenario, we consider $M_{N_3} > M_{N_2} \simeq M_{N_1}$. Therefore, resonance condition is satisfied only for the two lightest RH neutrinos N_2 and N_1. Hence we can neglect the contribution of N_3 in the CP asymmetry parameter (Eq. (25)) by

[5] Since the decay of N_i occurred before EWSB when all SM particles were massless and hence the phase space factor is equal to unity.

considering the summation over only N_1 and N_2 (i.e. $j = 1, 2$). Using the resonance condition in Eq. (26), one can easily notice that $S_j \sim \mathcal{O}\left(\frac{M_{N_j}}{\Gamma_j}\right) >> 1$ ($j = 1, 2$) and

$$\varepsilon_i \simeq -\sum_{j\neq i,\ j=1}^{2} \frac{M_{N_i}}{M_{N_j}} \frac{\Gamma_j}{M_{N_j}} S_j \frac{\mathrm{Im}\left[(\mathcal{M}_{\mathcal{D}}\mathcal{M}_{\mathcal{D}}{}^{\dagger})^2_{ij}\right]}{(\mathcal{M}_{\mathcal{D}}\mathcal{M}_{\mathcal{D}}{}^{\dagger})_{ii}\,(\mathcal{M}_{\mathcal{D}}\mathcal{M}_{\mathcal{D}}{}^{\dagger})_{jj}}\,, \tag{29}$$

where we have neglected the quantity V_j which is, in the present condition ($M_{N_2} - M_{N_1} \simeq \frac{\Gamma_1}{2}$), much smaller compared to S_j. The resonance condition leads to

$$\begin{aligned}
\Delta M^2_{21} &= M^2_{N_2} - M^2_{N_1}\,, \\
&= \frac{\Gamma_1}{2}\left(2\,M_{N_1} + \frac{\Gamma_1}{2}\right)\,, \\
&\simeq M_{N_1}\,\Gamma_1 + \mathcal{O}\left(\Gamma^2_1\right)\,.
\end{aligned} \tag{30}$$

Using Eq. (30) in Eq. (26) we get,

$$\begin{aligned}
S_1 &\simeq -\frac{M^2_{N_1}}{2\,M_{N_2}\,\Gamma_1}\,, \\
S_2 &\simeq \frac{M^2_{N_2}}{M_{N_1}}\frac{\Gamma_1}{\Gamma^2_1+\Gamma^2_2}\,.
\end{aligned} \tag{31}$$

Now, substituting the expressions of S_1 and S_2 in Eq. (29) and using $\mathrm{Im}\left[(\mathcal{M}_{\mathcal{D}}\mathcal{M}_{\mathcal{D}}{}^{\dagger})^2_{12}\right] = -\,\mathrm{Im}\left[(\mathcal{M}_{\mathcal{D}}\mathcal{M}_{\mathcal{D}}{}^{\dagger})^2_{21}\right]$, one obtains,

$$\varepsilon_2 \simeq -\frac{1}{2}\frac{\mathrm{Im}\left[(\mathcal{M}_{\mathcal{D}}\mathcal{M}_{\mathcal{D}}{}^{\dagger})^2_{12}\right]}{(\mathcal{M}_{\mathcal{D}}\mathcal{M}_{\mathcal{D}}{}^{\dagger})_{11}\,(\mathcal{M}_{\mathcal{D}}\mathcal{M}_{\mathcal{D}}{}^{\dagger})_{22}}\,, \tag{32}$$

$$\varepsilon_1 \simeq -\frac{\Gamma_1\,\Gamma_2}{\Gamma^2_1+\Gamma^2_2}\,\frac{\mathrm{Im}\left[(\mathcal{M}_{\mathcal{D}}\mathcal{M}_{\mathcal{D}}{}^{\dagger})^2_{12}\right]}{(\mathcal{M}_{\mathcal{D}}\mathcal{M}_{\mathcal{D}}{}^{\dagger})_{11}\,(\mathcal{M}_{\mathcal{D}}\mathcal{M}_{\mathcal{D}}{}^{\dagger})_{22}}\,, \tag{33}$$

$$\simeq \frac{2\,\Gamma_1\,\Gamma_2}{\Gamma^2_1+\Gamma^2_2}\,\varepsilon_2\,. \tag{34}$$

In the LP of Fig. 5, we show the variation of CP asymmetry parameter ε_1, generated from the decay of RH neutrino N_1, with the mass of N_1. Here we see that for the considered ranges of M_{N_1} ($1000\,\mathrm{GeV} \leq M_{N_1} \leq 3000\,\mathrm{GeV}$) and other relevant Yukawa couplings (see Eq. (23)), the CP asymmetry parameter ε_1 can be as large as $\sim 10^{-2}$, which is significantly large compared to ε_1 in the "normal" Leptogenesis case ($\varepsilon_1 \sim 10^{-8}$ for $M_{N_1} \sim 10^{10}$ GeV) [48]. In the RP of Fig. 5, we plot the variation of total decay width of N_1 with M_{N_1}. From this plot, one can easily notice that in the present scenario, Γ_1 lies between $\sim 10^{-12}$ GeV to 10^{-9} GeV for the entire considered range of M_{N_1}. All the points in both panels satisfy the neutrino oscillations data in the 3σ range

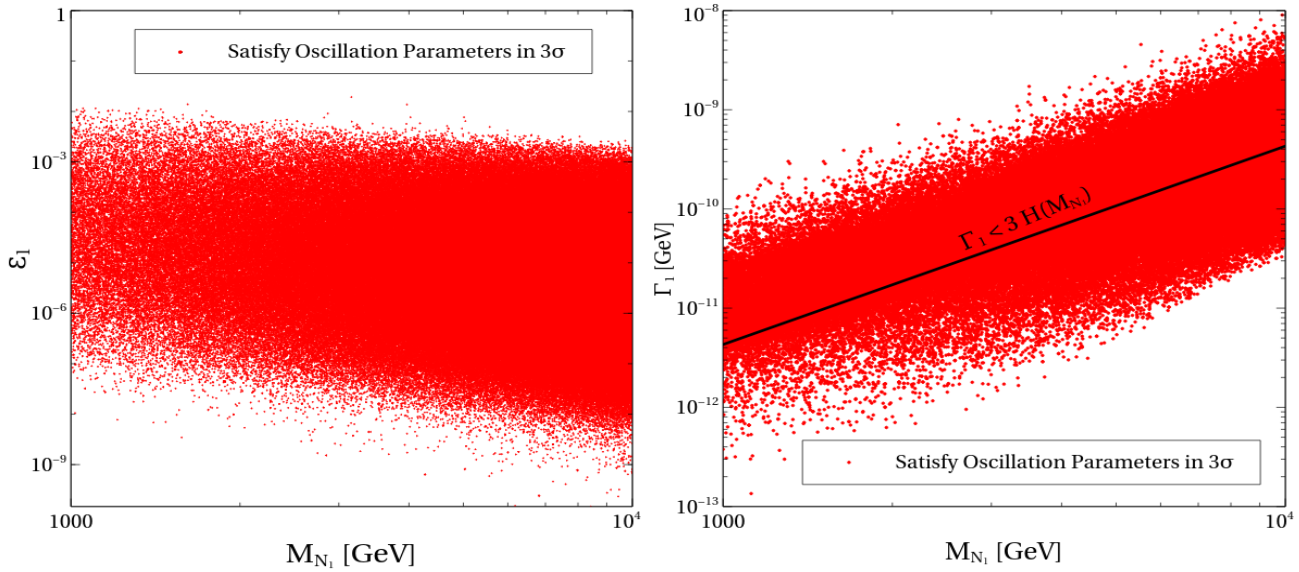

Figure 5: **LP:** Variation of CP asymmetry parameter ε_1 with the mass of N_1. **RP:** Variation of total decay width of N_1 with M_{N_1}. Black solid line represents the upper bound of Γ_1 coming from out of equilibrium condition of N_1. All the points in both plots satisfy the neutrino oscillation data in 3σ range.

while the black solid line in the RP provides the upper bound on Γ_1, obtained from the out of equilibrium conditions for N_1 i.e. $\Gamma_1 < 3\,H(M_{N_1})$ where H is Hubble parameter at $T = M_{N_1}$.

Next, we calculate the B − L asymmetry generated from the decays as well as the pair annihilations of the RH neutrinos N_1 and N_2. In order to calculate the net B − L asymmetry produced from the interactions of N_1 and N_2 at temperature of the Universe $T \simeq 150$ GeV (freeze-out temperature of sphaleron) we have to solve a set of three coupled Boltzmann equations. The relevant Boltzmann equations [48, 50] for calculating Y_{N_i} and Y_{B-L} are given below,

$$\frac{dY_{N_1}}{dz} = -\frac{M_{pl}}{1.66\,M_{N_1}^2}\frac{z\sqrt{g_\star(z)}}{g_s(z)}\langle\Gamma_1\rangle\left(Y_{N_1}-Y_{N_1}^{\rm eq}\right) - \frac{2\,\pi^2}{45}\frac{M_{pl}\,M_{N_1}}{1.66}\frac{\sqrt{g_\star(z)}}{z^2}\times \left(\langle\sigma{\rm v}\rangle_{N_1,\,Z_{BL}} + \langle\sigma{\rm v}\rangle_{N_1,t,H_{\rm BL}}\right)\left(Y_{N_1}^2-(Y_{N_1}^{\rm eq})^2\right), \tag{35}$$

$$\frac{dY_{N_2}}{dz} = -\frac{M_{pl}}{1.66\,M_{N_1}^2}\frac{z\sqrt{g_\star(z)}}{g_s(z)}\langle\Gamma_2\rangle\left(Y_{N_2}-Y_{N_2}^{\rm eq}\right) - \frac{2\,\pi^2}{45}\frac{M_{pl}\,M_{N_1}}{1.66}\frac{\sqrt{g_\star(z)}}{z^2}\times \left(\langle\sigma{\rm v}\rangle_{N_2,\,Z_{BL}} + \langle\sigma{\rm v}\rangle_{N_2,t,H_{\rm BL}}\right)\left(Y_{N_2}^2-(Y_{N_2}^{\rm eq})^2\right), \tag{36}$$

$$\frac{dY_{B-L}}{dz} = -\frac{M_{pl}}{1.66\,M_{N_1}^2}\frac{z\sqrt{g_\star(z)}}{g_s(z)}\left[\sum_{j=1}^{2}\left(\frac{Y_{B-L}}{2}\frac{Y_{N_j^{eq}}}{Y_L^{\rm eq}}+\varepsilon_j\left(Y_{N_j}-Y_{N_j^{eq}}\right)\right)\langle\Gamma_j\rangle\right], \tag{37}$$

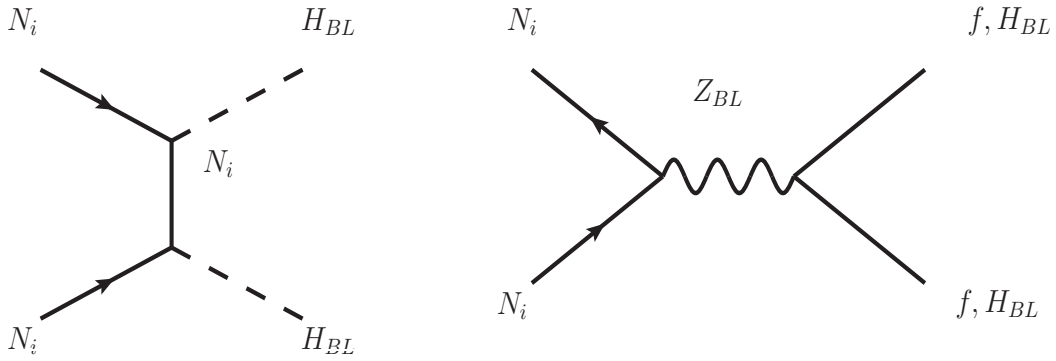

Figure 6: Feynman diagrams for the annihilations of RH neutrinos.

where $Y_X = \dfrac{n_X}{\mathrm{s}}$ denotes the comoving number density of X, with n_X being the actual number density and $z = \dfrac{M_{N_1}}{T}$. Planck mass is denoted by M_{pl}. The quantity $g_\star(z)$ is a function of g_ρ and g_s, the effective degrees of freedom related to the energy and entropy densities of the Universe respectively, and it has the following expression [64],

$$\sqrt{g_\star(z)} = \frac{g_{\mathrm{s}}(z)}{\sqrt{g_\rho(z)}} \left(1 - \frac{1}{3}\frac{\mathrm{d}\ln g_{\mathrm{s}}(z)}{\mathrm{d}\ln z}\right) . \tag{38}$$

Before EWSB, the variation of $g_s(z)$ with respect to z is negligible compared to the first term within the brackets and hence one can use $\sqrt{g_\star(z)} \simeq \dfrac{g_{\mathrm{s}}(z)}{\sqrt{g_\rho(z)}}$. The equilibrium comoving number density of X $(X = N_i, L)$, obeying the Maxwell Boltzmann distribution, is given by [64]

$$Y_X^{\mathrm{eq}}(z) = \frac{45\, g_X}{4\,\pi^4} \left(\frac{M_X\, z}{M_{N_1}}\right)^2 \frac{\mathrm{K}_2\left(\frac{M_X}{M_{N_1}}\, z\right)}{g_s\left(\frac{M_{N_1}}{z}\right)} , \tag{39}$$

where g_X and M_X are the internal degrees of freedom and mass of X respectively while $g_s\left(\frac{M_{N_1}}{z}\right)$ is the effective degrees of freedom related to the entropy density of the Universe at temperature $T = \dfrac{M_{N_1}}{z}$. $\mathrm{K}_2\left(\frac{M_X}{M_{N_1}}\, z\right)$ is the modified Bessel function of order 2. The relevant Feynman diagrams including both decay and annihilation of N_i are shown in Figs. 4 and 6. The expression of thermal averaged decay width $\langle\Gamma_i\rangle$, which is related to total decay width Γ_i of N_i is given as

$$\langle\Gamma_i\rangle = \Gamma_i \; \frac{\mathrm{K}_1\left(\frac{M_{N_i}}{M_{N_1}}\, z\right)}{\mathrm{K}_2\left(\frac{M_{N_i}}{M_{N_1}}\, z\right)} . \tag{40}$$

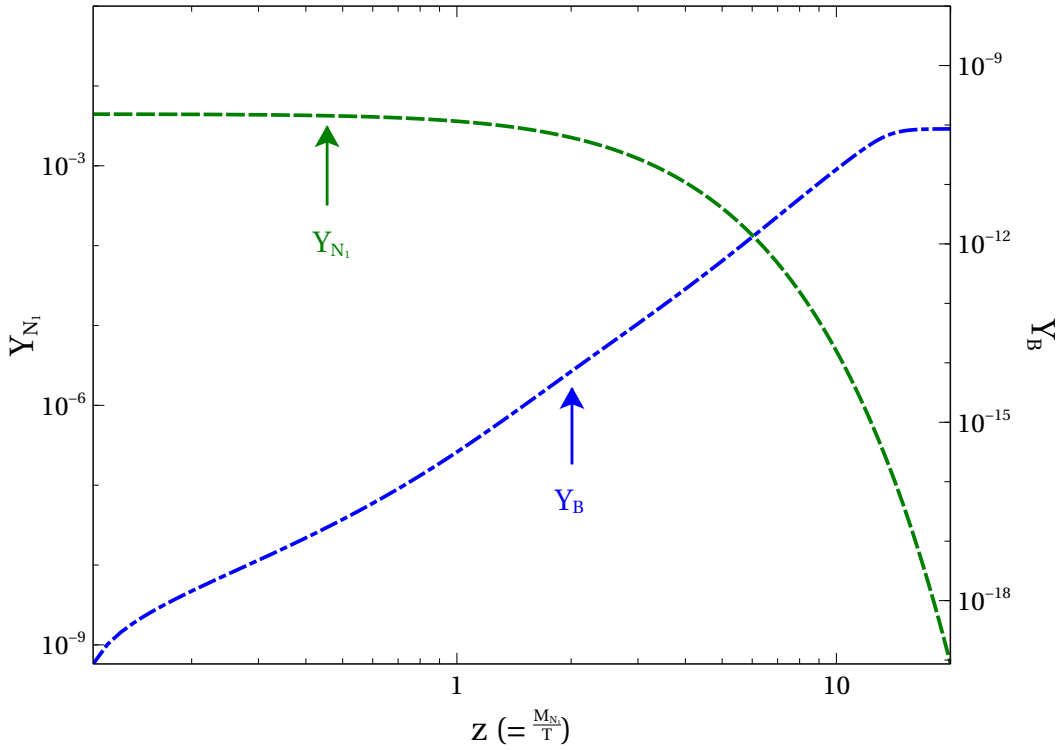

Figure 7: Variation of Y_{N_1} (Green dash line) and Y_{B-L} (blue dash-dot line) with z where other parameters have kept fixed at $M_{N_1} = 2000$ GeV, $\alpha_{BL}\left(= \frac{g_{BL}^2}{4\pi}\right) = 3 \times 10^{-4}$, $M_{Z_{BL}} = 3000$ GeV.

The thermally average annihilation cross sections $\langle \sigma \mathrm{v} \rangle_{N_i, Z_{BL}}$ and $\langle \sigma \mathrm{v} \rangle_{N_i, Z_{BL}}$, appearing in Boltzmann equations (Eqs. (35) and (36)) for the processes shown in Fig. 6, can be defined in a generic form,

$$\langle \sigma \mathrm{v} \rangle_{N_i, x} = \frac{z}{16\, M_{N_i}^4\, M_{N_1}\, g_{N_i}^2\, \mathrm{K}_2\left(\frac{M_{N_i}}{M_{N_1}}\, z\right)^2} \int_{4\, M_{N_i}^2}^{\infty} \hat{\sigma}_{N_i, x}\, \mathrm{K}_1\left(\frac{\sqrt{s}}{M_{N_1}}\, z\right)\, \sqrt{s}\, ds\,, \tag{41}$$

where the $\hat{\sigma}_{N_i, x}$ is related to the actual annihilation cross section $\sigma_{N_i, x}$ by the following relation

$$\hat{\sigma}_{N_i, x} = 2\, g_{N_i}^2\, \left(s - 4\, M_{N_1}^2\right)\, \sigma_{N_i, x}\,, \tag{42}$$

where $g_{N_i} = 2$ is the internal degrees of freedom of RH neutrino N_i. The expression of $\hat{\sigma}_{N_i, Z_{BL}}$ and $\hat{\sigma}_{N_i, t, H_{BL}}$ for the present model is given in Ref. [50].

To calculate the B − L asymmetry at around $T \simeq 150$ GeV, we have to numerically solve the set of three coupled Boltzmann equations (Eqs. (35)-(37)) using Eqs. (38)-(42). However, we can reduce the two flavour analysis (when both N_2 and N_1 are separately considered) into one

flavour case by considering the parameters of $\mathcal{M}_{\mathcal{D}}$ matrix in such a way so that the decay widths of N_1 and N_2 are of the same order i.e. $\Gamma_1 \sim \Gamma_2$. Hence, the CP asymmetry generated from the decays of both N_1 and N_2 are almost identical ($\varepsilon_1 \sim \varepsilon_2$, see Eq. (32)-(33)). In this case, the net B − L asymmetry is equal to twice of that is being generated from the CP violating interactions of the lightest RH neutrino N_1 [50]. Hence instead of solving three coupled differential equations we now only need to solve Eqs. (35) and (37). The results we have found by numerically solving Eqs. (35) and (37) are plotted in Fig. 7. In this plot, we have shown the variation of Y_{N_1} and Y_{B-L} with z for $M_{N_1} = 2000$ GeV, $\alpha_{BL} = 3 \times 10^{-4}$ and $M_{Z_{BL}} = 3000$ GeV. While solving the coupled Boltzmann equations we have considered the following initial conditions: $Y_{N_1}(T_{\rm in}) = Y^{\rm eq}_{N_1}$ and $Y_{B-L} = 0$ with $T_{\rm in}$ is the initial temperature which we have taken as 20 TeV. Thereafter, the evolutions of Y_{N_1} and Y_{B-L} are governed by their respective Boltzmann equations. From Fig. 7, one can notice that initially upto $z \sim 1$ ($T \sim M_{N_1}$), the comoving number density of Y_{N_1} does not change much as a result of the B − L asymmetry produced from the decay, and the annihilation of N_1 is also less. However, as the temperature of the Universe drops below the mass of M_{N_1}, there is a rapid change in the number density of N_1, which changes around six orders of magnitude between $z = 1$ and $z = 20$. Consequently, the large change in Y_{N_1} significantly enhances the B − L asymmetry Y_{B-L} and finally Y_{B-L} saturates to the desired value around $\sim 10^{-10}$, when there are practically no N_1 left to produce any further B − L asymmetry.

The produced $B-L$ asymmetry is converted to net baryon asymmetry of the Universe through the sphaleron transitions while they are in equilibrium with the thermal bath. The quantities Y_{B-L} and Y_B are related by the following equation [46]

$$Y_B = -\,2 \times \frac{28}{79}\, Y_{B-L}(T_{\rm f})\,, \tag{43}$$

where $T_{\rm f} \simeq 150$ GeV is the temperature of the Universe upto which the sphaleron process, converting $B - L$ asymmetry to a net B asymmetry, maintains its thermal equilibrium. The extra factor of two in the above equation is due to the equal contribution to Y_{B-L} arising from the CP violating interactions of N_2 as well. Finally, we calculate the net baryon asymmetry Y_B for three different masses of RH neutrino N_1 and CP asymmetry parameter ε_1. The results are listed in Table II. In all three cases, the final baryon asymmetry lies within the experimentally observed range for Y_B i.e. $(8.239 - 9.375) \times 10^{-11}$ at 95% C.L. [41].

C. FIMP Dark Matter

In the present section we explore the FIMP scenario for dark matter in the Universe, by considering the real scalar field ϕ_{DM} as a corresponding candidate. As described in the Section II, the unbroken $\mathbb{Z}_2$ parity of ϕ_{DM} makes the scalar field absolutely stable over the cosmological time scale and hence can play the role of a dark matter candidate. Since the B − L charge of

M_{N_1} [GeV]	ε_1	$Y_B = \frac{n_B}{S}$
1600	4.4×10^{-4}	8.7121×10^{-11}
1800	2.25×10^{-4}	8.7533×10^{-11}
2000	1.8×10^{-4}	8.5969×10^{-11}

Table II: Baryon asymmetry of the Universe generated for three different values of M_{N_1} and ε_1.

ϕ_{DM} is zero, therefore DM talks to the SM as well as the BSM particles only via the two Higgs bosons present in the model, one is the SM-like Higgs h_1 while other one is the BSM Higgs h_2. The corresponding coupling strengths, in terms of mixing angle α and λs, are listed in Table III. As the FIMP never enters into thermal equilibrium, these couplings have to be extremely feeble in order to make the corresponding interactions nonthermal. Due to the nonthermal nature, the initial number density of FIMP is assumed to be negligible and as the temperature of the Universe begins to fall down, they start to be produced dominantly from the decays of other heavy particles. In principle, the FIMP can also be produced from the scattering of particles in the thermal bath, however the rate of such processes are subdominant compared to that from decay.

Vertex $a\,b\,c$	Vertex Factor g_{abc}
$\phi_{DM}\,\phi_{DM}\,h_1$	$-2\left(\lambda_{Dh} v \cos\alpha + \lambda_{DH} v_{BL} \sin\alpha\right)$
$\phi_{DM}\,\phi_{DM}\,h_2$	$2\left(\lambda_{Dh} v \sin\alpha - \lambda_{DH} v_{BL} \cos\alpha\right)$

Table III: Couplings of FIMP (ϕ_{DM}) with h_1 and h_2.

In the present scenario, we have considered all the particles except ϕ_{DM} to be in thermal equilibrium. Before EWSB, all the SM particles are massless. In this regime, production of ϕ_{DM} occurs mainly from the decay and/or annihilation of BSM particles namely H_{BL}, N_i and Z_{BL}. Also, before EWSB the annihilation of all four scalar fields (one charged scalar and two real scalars) of the SM Higgs doublet ϕ_h, which are although massless, can produce ϕ_{DM} . Feynman diagrams for all the production processes of ϕ_{DM} before EWSB are shown in Fig. 8.

After EWSB, all the SM particles become massive and consequently besides the BSM particles, ϕ_{DM} can now also be produced from the decay and/or annihilation of the SM particles as well. The corresponding Feynman diagrams are shown in Fig. 9. In generating the vertex factors for

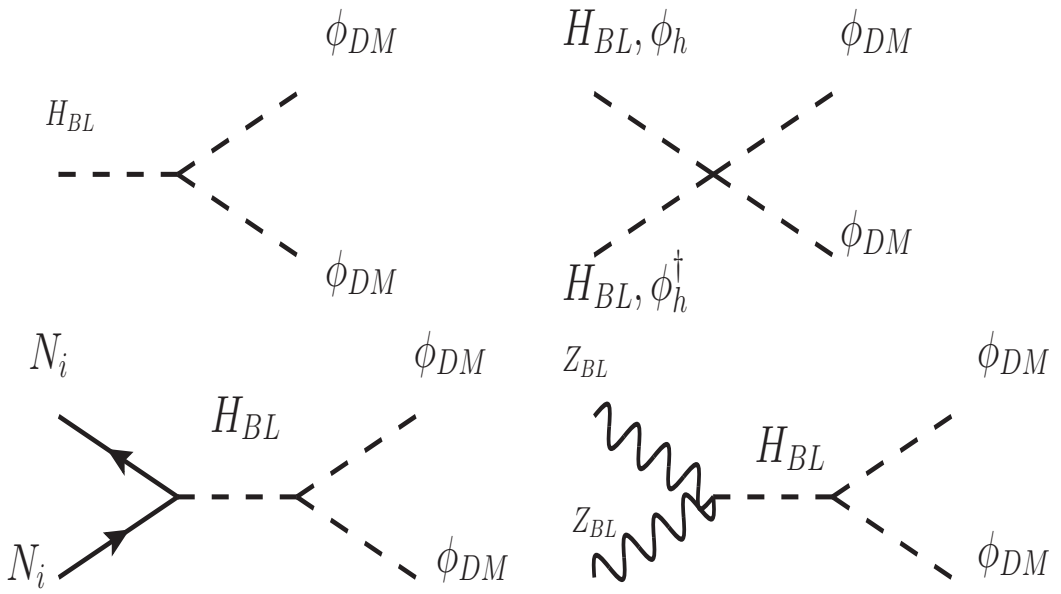

Figure 8: Feynman diagrams for the all possible production modes of ϕ_{DM} before EWSB.

different vertices to compute the Feynman diagrams as listed in Fig. 8 and Fig. 9 we have used the LanHEP [66] package.

In order to compute the relic density of a species at the present epoch, one needs to study the evolution of the number density of the corresponding species with respect to the temperature of the Universe. The evolution of the number density of ϕ_{DM} is governed by the Boltzmann equation containing all possible number changing interactions of ϕ_{DM}. The Boltzmann equation of ϕ_{DM} in terms of its comoving number density $Y_{\phi_{DM}} = \frac{n_{\phi_{DM}}}{\mathrm{s}}$, where n and s are actual number density and entropy density of the Universe is given by

$$\begin{aligned}\frac{dY_{\phi_{DM}}}{dz} = &\frac{2M_{pl}}{1.66M_{h_1}^2}\frac{z\sqrt{g_\star(z)}}{g_s(z)}\left[\sum_{i=1,\,2}\langle\Gamma_{h_i\to\phi_{DM}\phi_{DM}}\rangle(Y_{h_i}^{\rm eq}-Y_{\phi_{DM}})\right]\\ &+\frac{4\pi^2}{45}\frac{M_{pl}M_{h_1}}{1.66}\frac{\sqrt{g_\star(z)}}{z^2}\left[\sum_p\langle\sigma{\rm v}_{p\bar{p}\to\phi_{DM}\phi_{DM}}\rangle(Y_p^{\rm eq\ 2}-Y_{\phi_{DM}}^2)\right.\\ &\left.+\langle\sigma{\rm v}_{h_1h_2\to\phi_{DM}\phi_{DM}}\rangle(Y_{h_1}^{\rm eq}Y_{h_2}^{\rm eq}-Y_{\phi_{DM}}^2)\right],\end{aligned} \tag{44}$$

where $z = \frac{M_{h_1}}{T}$, while $\sqrt{g_\star(z)}$, $g_s(z)$ and M_{pl} are same as those in Eqs. (35)–(37) of Section III B. In the above equation (Eq. (44)), first term represents the contribution coming from the decays of h_1 and h_2. The expressions of equilibrium number density $Y_X^{\rm eq}(z)$ (X is any SM or BSM particle expect ϕ_{DM}) and the thermal averaged decay width $\langle\Gamma_{h_i\to\phi_{DM}\phi_{DM}}\rangle$ can be obtained from Eqs. (39)

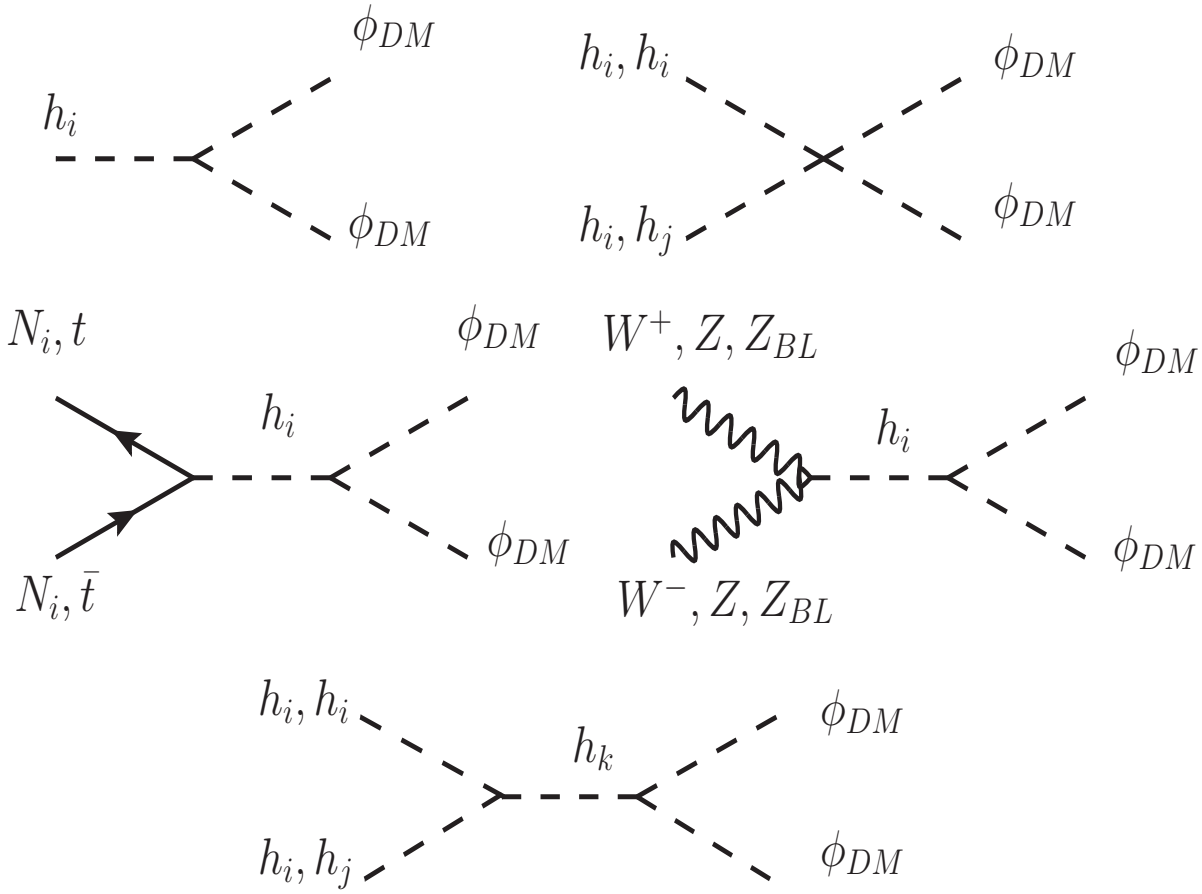

Figure 9: Production processes of ϕ_{DM} from both SM as well as BSM particles after EWSB.

and (40), respectively by only replacing M_{N_1} with M_{h_1}. As mentioned above, the summation in the first terms is valid only after EWSB when both h_1 and h_2 are contributing to the relic density of ϕ_{DM}, otherwise the summation over i is replaced by $i = 2$ only. The dark matter production from the pair annihilations of SM and BSM particles are described by the second term of the Boltzmann equation. Here, summation over p includes all possible pair annihilation channels namely W^+W^-, ZZ, $Z_{BL}Z_{BL}$, N_iN_i, h_ih_i, $t\bar{t}$. However before EWSB, pair annihilations of only the BSM particles contribute to the production processes (i.e. $p = Z_{BL}$, N_i, H_{BL} , see Fig. 8). The third term, which is present only after EWSB, is another the production mode of ϕ_{DM} from the annihilation of h_1 and h_2. The expressions of all the relevant cross sections and decay widths for computing the DM number density are given in Appendix D. The most general form of thermally averaged annihilation cross section for two different annihilating particles of mass

M_A and M_B is given by [40],

$$
\begin{aligned}
f_1 &= \sqrt{s^2 + (M_A^2 - M_B^2)^2 - 2\,s\,(M_A^2 + M_B^2)}\,, \\
f_2 &= \sqrt{s - (M_A - M_B)^2}\,\sqrt{s - (M_A + M_B)^2}\,, \\
\langle \sigma v_{A\,B \to \phi_{DM}\phi_{DM}} \rangle &= \frac{1}{8\,M_A^2\,M_B^2\,T\,\mathrm{K}_2\left(\frac{M_A}{T}\right)\,\mathrm{K}_2\left(\frac{M_B}{T}\right)} \times \\
&\quad \int_{(M_A+M_B)^2}^{\infty} \frac{\sigma_{A\,B \to \phi_{DM}\phi_{DM}}}{\sqrt{s}}\,f_1\,f_2\,\mathrm{K}_1\left(\frac{\sqrt{s}}{T}\right)\,\mathrm{d}s\,.
\end{aligned}
\tag{45}
$$

Finally, the relic density of ϕ_{DM} is obtained using the following relation between Ωh^2 and $Y_{\phi_{DM}}(0)$ [63–65],

$$
\Omega h^2 = 2.755 \times 10^8 \left(\frac{M_{DM}}{\mathrm{GeV}}\right)\,Y_{\phi_{DM}}(0)\,,
\tag{46}
$$

where $Y_{\phi_{DM}}(0)$ is the value of comoving number density at the present epoch, which can be obtained by solving the Boltzmann equation.

In the left panel (LP) and right panel (RP) of Fig. 10, we have shown the variation of DM relic density with z. In LP, we have shown the dependence of DM relic density with the initial temperature[6]. We can clearly see from the figure that as long as the initial temperature is above the mass of BSM Higgs ($M_{h_2} \sim 500$ GeV), final relic density does not depend on the choice of the initial temperature and reproduces the observed DM relic density of the Universe for the set of parameters value as written in the caption. If we reduce the initial temperature from 500 GeV, i.e. for $T_{in} = 251$ GeV, the decay contribution of BSM Higgs h_2 becomes less since corresponding the number density of h_2 for $T_{in} < M_{h_2}$ is Boltzmann suppressed (exponentially suppressed), which is clearly shown by the blue dashed-dotted line. Hence, if we reduce the initial temperature (T_{in}) further i.e. $T_{in} < M_{h_2}, M_{h_1} \sim 42$ GeV then the number densities of both SM-like Higgs h_1 as well as BSM Higgs h_2 become Boltzmann suppressed and hence, less amount of DM production will take place which is evident from the LP of Fig. 10 (represented by the yellow dashed-dot line). On the other hand in the RP of Fig. 10, we have shown the contributions to DM relic density coming from decay and annihilation. Magenta dotted horizontal line represents the present day observed DM relic density of the Universe. Green dashed line represents the total decay contribution arising from the decays of both h_1 and h_2 whereas the net annihilation contribution coming from the annihilation of all SM as well as BSM particles, has been shown by the blue dashed-dotted line. There is a sudden rise in the annihilation contribution which

[6] Initial temperature (T_{in}) is the temperature upto which we have assumed the number density of dark matter is zero and production processes start thereafter.

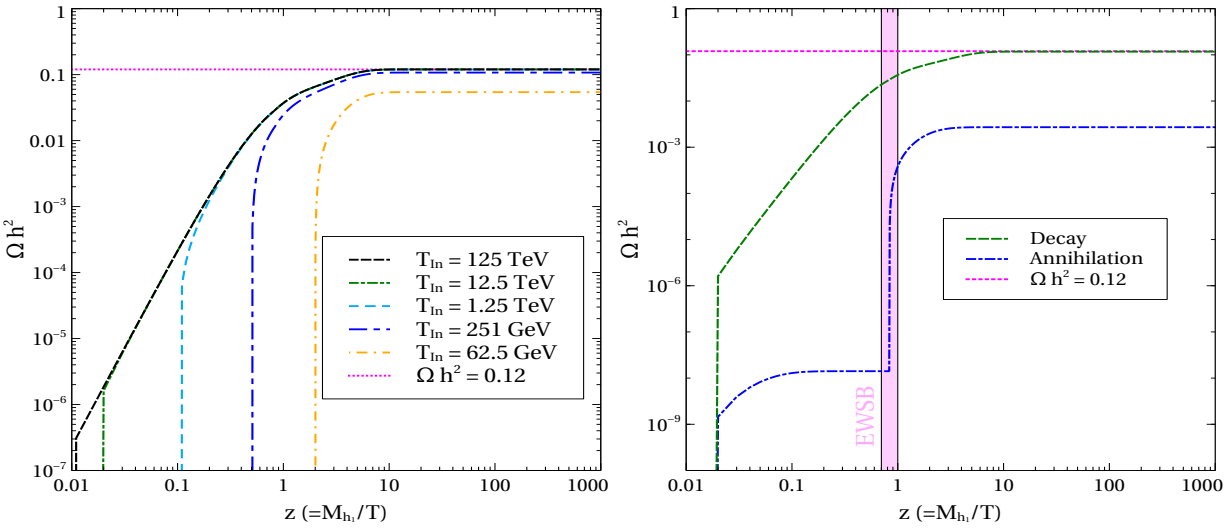

Figure 10: Left (Right) panel: Variation of relic density Ωh^2 with z for different initial temperature (contributions to Ωh^2 coming from decay and annihilation), where other parameters are fixed at $\lambda_{Dh} = 8.75 \times 10^{-13}$, $\lambda_{DH} = 5.88 \times 10^{-14}$, $M_{DM} = 50$ GeV, $M_{Z_{BL}} = 3000$ GeV, $g_{BL} = 0.07$, $M_{h_1} = 125.5$ GeV and $M_{h_2} = 500$ GeV, $\alpha = 10^{-4}$.

occurs around the Universe temperature $T \sim 154$ GeV (i.e. EWSB temperature). After the EWSB temperature, all the SM particles become massive and hence the sudden rise in the annihilation part because of the appearance of the following annihilation channels $W^+ W^-$, $Z Z$, $h_1 h_1$, $h_1 h_2$. The plot clearly implies that the lion share of the contribution comes from the decay of both Higgses h_1 and h_2, while for the considered values of model parameters the annihilation contribution is subdominant.

In the LP of Fig. 11, we have shown how the individual decay contribution from each scalar varies with z. Here we consider the following values of the scalar quartic couplings $\lambda_{Dh} = 8.75 \times 10^{-13}$ and $\lambda_{DH} = 5.88 \times 10^{-14}$. From this plot we can see that before EWSB SM-like Higgs h_1, being massless, cannot decay. In this regime only the decay of BSM Higgs h_2 contributes, while after EWSB even the SM-like Higgs starts contributing to the DM production and hence we get an increased relic density (right side of EWSB). Its worth mentioning here that while generating the plot in the LP of Fig. 11, we have taken the scalar quartic couplings λ_{Dh} and λ_{DH} of different strengths such that the contributions of both the scalars (h_1 and h_2) to the DM relic density are of equal order. This is because for the case of BSM Higgs h_2 decay the coupling λ_{DH} multiplied by the B $-$ L symmetry breaking VEV v_{BL} is relevant, while for the decay of the SM-like Higgs h_1, the product of the parameter λ_{Dh} and the EWSB VEV v is relevant. Since in the present case $v_{BL} > v$, the magnitudes of the two quartic couplings λ_{Dh} and λ_{DH} are of different order (see Table III). On the other hand, in the RP of Fig. 11, we have

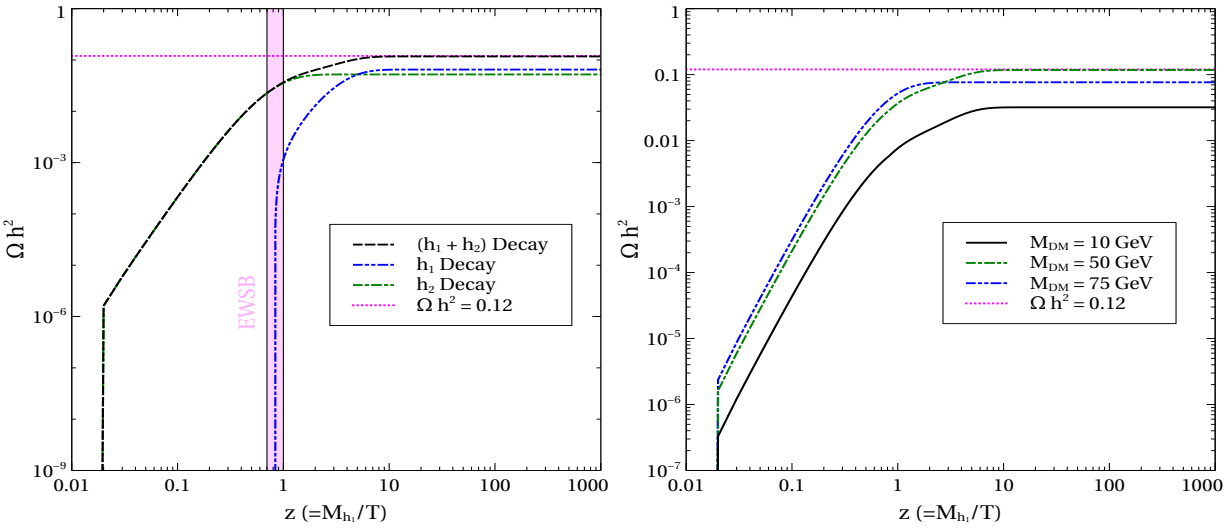

Figure 11: Left panel: Showing variation of decay contributions of both the Higgs bosons to Ωh^2 separately with z. Right panel: Variation of relic density Ωh^2 with z for different values of DM mass M_{DM}. Other parameters value have been kept fixed at $\lambda_{Dh} = 8.75 \times 10^{-13}$, $\lambda_{DH} = 5.88 \times 10^{-14}$, M_{DM} = 50 GeV (for LP), $M_{Z_{BL}} = 3000$ GeV, $g_{BL} = 0.07$, $M_{h_1} = 125.5$ GeV and $M_{h_2} = 500$ GeV, $\alpha = 10^{-4}$.

shown the variation of the relic density with z for three different values of the DM mass M_{DM}. From Eq. (46), one can see that the DM relic density is directly proportional to the mass M_{DM} and as a result when other relevant couplings remain unchanged Ωh^2 increases with M_{DM}. This feature is clearly visible in the RP for the cases with $M_{DM} = 10$ GeV (black solid line) and 50 GeV (green dashed line) respectively. However for $M_{DM} = 75$ GeV (blue dashed line), instead of rising, Ωh^2 decreases because for this value of DM mass the decay of h_1 to a pair of ϕ_{DM} becomes kinematically forbidden and hence, there is a reduction in DM relic density compared to the previous case with $M_{DM} = 50$ GeV.

In LP and RP of Fig. 12, we have shown how the relic density varies with z for different values of scalar quartic couplings λ_{Dh} and λ_{DH}, respectively. In each panel, one can easily notice that there exists a kink around the EWSB region. However in the LP, the kink occurs for a higher value of λ_{Dh} while in the RP, the situation is just opposite. We have already seen in the LP of Fig. 11 that before EWSB only h_2 decay is contributing to DM relic density and at the EWSB region SM-like Higgs h_1 also starts contributing. A kink will always appear in the relic density curve when contribution of the SM-like Higgs boson h_1 to Ωh^2 is larger compared to that of the BSM Higgs h_2 i.e. $\Gamma_{h_1 \to \phi_{DM}\phi_{DM}} > \Gamma_{h_2 \to \phi_{DM}\phi_{DM}}$. The values of scalar quartic couplings λ_{Dh} and λ_{DH} in the LP of Fig. 11 are such that $\Gamma_{h_2 \to \phi_{DM}\phi_{DM}}$ always remains large compared to $\Gamma_{h_1 \to \phi_{DM}\phi_{DM}}$ and hence no kink is observed in the total relic density curve. However, in the present figure (in both panels of Fig. 12) we do have kinks around the EWSB region, because in

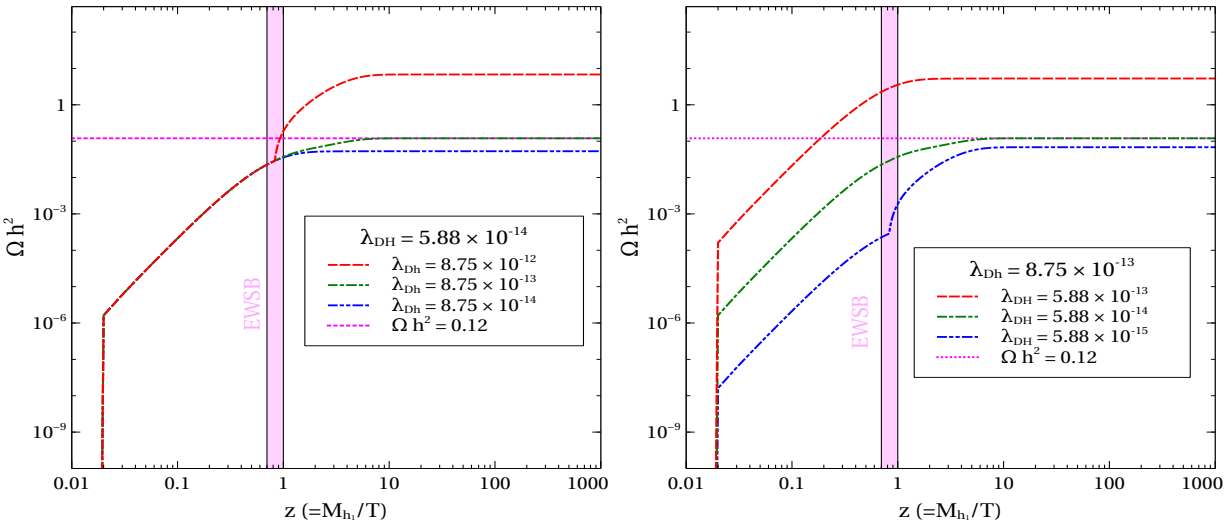

Figure 12: Left (Right) panel: Variation of relic density Ωh^2 with z for three different values of λ_{Dh} (λ_{DH}), where other parameters are fixed at $\lambda_{DH} = 5.88 \times 10^{-14}$ ($\lambda_{Dh} = 8.75 \times 10^{-13}$), $M_{DM} = 50$ GeV, $M_{Z_{BL}} = 3000$ GeV, $g_{BL} = 0.07$, $M_{h_1} = 125.5$ GeV and $M_{h_2} = 500$ GeV, $\alpha = 10^{-4}$.

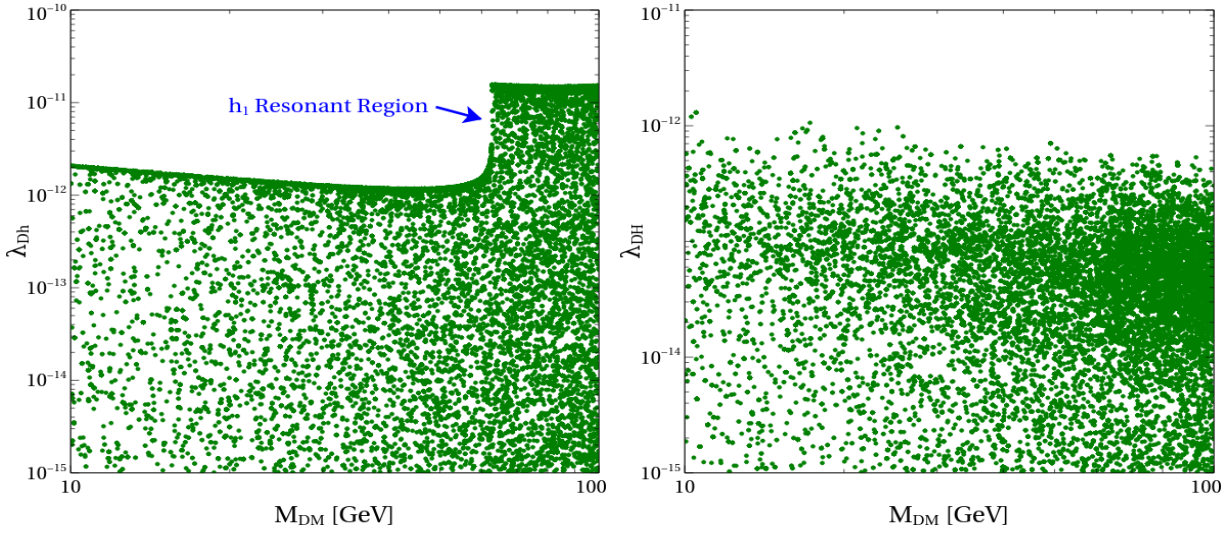

Figure 13: Left (Right) panel: Left (Right) panel: Allowed region in the $\lambda_{Dh} - M_{DM}$ ($\lambda_{DH} - M_{DM}$) plane where other parameters are fixed at $M_{Z_{BL}} = 3000$ GeV, $g_{BL} = 0.07$, $M_{h_1} = 125.5$.

the LP with $\lambda_{DH} = 5.88 \times 10^{-14}$, $\Gamma_{h_1 \to \phi_{DM}\phi_{DM}} > \Gamma_{h_2 \to \phi_{DM}\phi_{DM}}$ condition is satisfied only for the case with larger value of $\lambda_{Dh} = 8.75 \times 10^{-12}$ ($\lambda_{Dh} >> \lambda_{DH}$) while in the RP with a fixed value of $\lambda_{Dh} = 8.75 \times 10^{-13}$, the above condition is maintained only for the lesser value of λ_{DH} (i.e. $\lambda_{DH} = 5.88 \times 10^{-15}$).

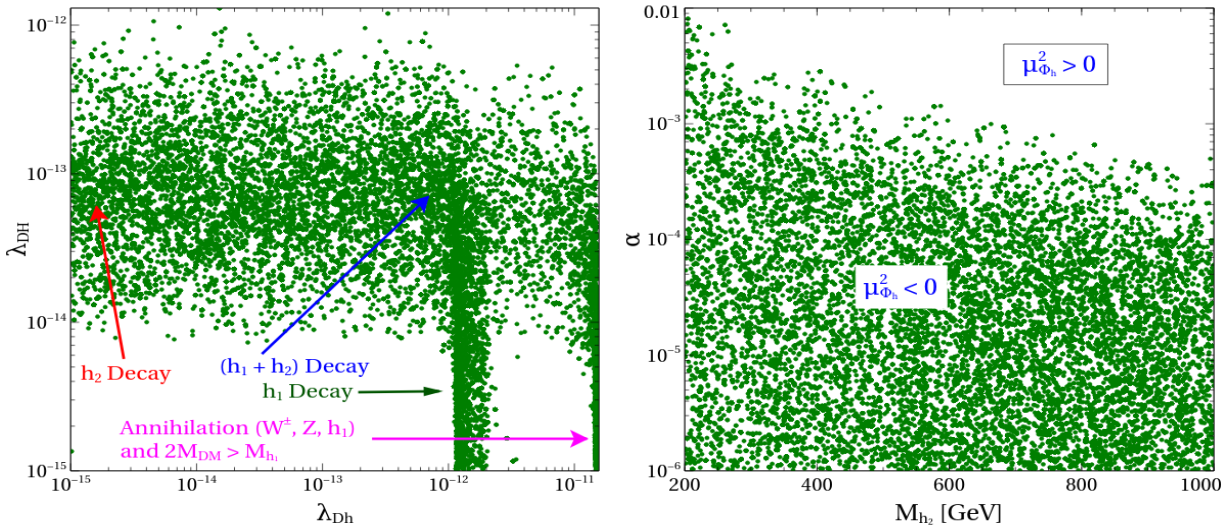

Figure 14: Left (Right) panel: Allowed region in the $\lambda_{Dh} - \lambda_{DH}$ ($M_{h_2} - \alpha$) plane where other parameters are fixed at $M_{Z_{BL}} = 3000$ GeV, $g_{BL} = 0.07$, $M_{h_1} = 125.5$.

In the LP of Fig. 13, we have shown the allowed in the $M_{DM} - \lambda_{Dh}$ plane, where all the points satisfy the relic density bound. We see a small slope of λ_{Dh} for $M_{DM} \leq 62.5$ GeV, this is because the DM relic density is proportional to its mass M_{DM}, hence to satisfy the relic density bound we need small λ_{Dh} for large M_{DM}. On the other hand, there is a sharp rise in the allowed values of λ_{Dh} at $M_{DM} = M_{h_1}/2$, because as $M_{DM} \to M_{h_1}/2$, the decay contribution of h_1 becomes very small (due to phase space suppression), hence to satisfy the relic density bound there is a rapid increase of λ_{Dh} and after that λ_{Dh} remains almost constant with the variation of M_{DM}. This is because as we mentioned earlier, after $M_{DM} > M_{h_1}/2$, the decay mode of h_1 to a pair of ϕ_{DM} becomes kinematically forbidden and therefore the coupling λ_{Dh} does not have any significant effect on Ωh^2 as in this regime with small value of mixing angle α, λ_{Dh} can affect the relic density only through its presence in the annihilation processes which have subdominant contribution to Ωh^2 (see RP of Fig. 10). However for $M_{DM} > M_{h_1}/2$, the annihilation processes will be important only for the larger value of λ_{Dh}. Thus all values of $\lambda_{Dh} \gtrsim 2 \times 10^{-11}$ are not allowed due to large contribution coming from the annihilation processes like W^+W^-, ZZ and h_1h_1. The allowed region corresponding to $\lambda_{DH} - M_{DM}$ plane is also shown in the RP of Fig. 13. Here like LP, no sharp rise exists because for the entire considered DM mass range 1 GeV $\leq M_{DM} \leq$ 100 GeV, DM production from h_2 decay never enters into the kinematically forbidden region i.e for 200 GeV $\leq M_{h_2} \leq$ 1000 GeV M_{DM} always remains less than $M_{h_2}/2$.

In the LP of Fig. 14, we have shown the allowed region in the coupling plane ($\lambda_{Dh} - \lambda_{DH}$) which reproduces the observed DM relic density ($0.1172 \leq \Omega h^2 \leq 0.1226$). In this figure, we have clearly indicated which region is dominated by what types of DM production processes i.e.

DM production from the decay of h_1 or h_2 or both or entirely from the annihilations of SM particles like $W^{\pm}$, Z, h_1 etc. One interesting point to note here is that, there exists a certain gap in the λ_{Dh} value in between 2×10^{-12} to 2×10^{-11} for $10^{-15} \leq \lambda_{DH} \leq 10^{-14}$. From LP of Fig. 13, we see that $\lambda_{Dh} \geq 2 \times 10^{-12}$ is allowed only for $M_{DM} \geq M_{h_1}/2$ where most of the contribution to DM relic density comes from the decay of h_2 as that of h_1 is now kinematically forbidden. Therefore, in the current plot (LP of Fig. 14) with smaller values of the coupling λ_{DH} ($10^{-15} \leq \lambda_{DH} \leq 10^{-14}$), the contribution of h_2 never attains to a desirable value which is required to reproduce the observed DM relic density. However, with the relatively larger value of λ_{Dh} ($\lambda_{Dh} \sim 2 \times 10^{-11}$) when annihilation processes become dominant one we get some allowed region in the $\lambda_{Dh} - \lambda_{DH}$ plane for $10^{-15} \leq \lambda_{DH} \leq 10^{-14}$. On the other hand, in the RP of Fig. 14 we have presented the allowed region in $M_{h_2} - \alpha$ plane after satisfying the relic density bound. From this figure one can see that with the increase of M_{h_2}, values of allowed mixing angle α decrease. The reason behind this decrement is related to the vacuum stability conditions as given in the Eq. (14). The region satisfying both the relic density bound as well as the vacuum stability conditions is shown by green dots while in the other part of $M_{DM} - \alpha$ plane $\mu^2_{\phi_h}$ becomes positive which is undesirable in our context.

IV. CONCLUSION

In this work we considered a local $\mathrm{U(1)_{B-L}}$ extension of the SM and to cancel the additional anomalies associated with this gauge symmetry we introduced three RH neutrinos (N_i, $i = 1$, 2, 3). Besides the three RH neutrinos, we also introduced two SM gauge singlet scalars ϕ_H and ϕ_{DM}. One of the scalars ϕ_H, being charged under $\mathrm{U(1)_{B-L}}$, takes a nonzero VEV and breaks the proposed $\mathrm{B-L}$ symmetry spontaneously. Although the other scalar field ϕ_{DM} has no $\mathrm{B-L}$ charge, it is made stable by making it odd under a $\mathbb{Z}_2$ parity. It hence acts as a dark matter candidate. After spontaneous breaking of $\mathrm{U(1)_{B-L}}$ gauge symmetry, all RH neutrinos and extra neutral gauge boson Z_{BL}, acquired mass. Due to the presence of the three RH neutrinos in the model, we easily generated Majorana masses for the three light neutrinos by the Type I seesaw mechanism. This model is also able to explain baryogenesis via leptogenesis, where we generated the lepton asymmetry in the Universe from out of equilibrium, CP violating decays of two degenerate RH neutrinos and converted this lepton asymmetry to the observed baryon asymmetry through the sphaleron transitions.

In explaining the neutrino masses by Type I seesaw mechanism, we considered a complex Dirac mass matrix $\mathcal{M}_{\mathcal{D}}$ and a diagonal Majorana mass matrix $\mathcal{M}_{\mathcal{R}}$ for the RH neutrinos. In determining the allowed model parameter space, we used the measured values of neutrino oscillation parameters namely three mixing angles (θ_{12}, θ_{13} and θ_{23}) and two mass square differences (Δm^2_{21}, Δm^2_{atm}) in their current 3σ range. In particular, in the current model we could reproduce

the whole allowed 3σ range of the neutrino oscillation parameters by different combinations of the relevant model parameters. The Dirac CP phase was constrained to lie within two distinct regions. One is the entire first quadrant ($0^\circ - 90^\circ$) while the other one spans the entire fourth quadrant ($270^\circ - 360^\circ$). However, if we considered the T2K result on Dirac CP phase then the values of δ lying in the fourth quadrant are more favourable compared to those in the first quadrant. We also computed the magnitudes of the Jarlskog invariant $J_{\rm CP}$ and found that the values of $J_{\rm CP}$, for the model parameters which satisfy neutrino oscillation data, always lie below 0.039. Finally, we calculated the values of $m_{\beta\beta}$, the quantity relevant to neutrino less double β decay, for the allowed model parameter space.

Since we allowed complex Yukawa couplings in the Dirac mass matrix $\mathcal{M}_{\mathcal{D}}$, the decays of RH neutrinos were CP violating. We took the masses of the RH neutrinos in the TeV range and worked in the parameter space where the lightest two RH neutrino states were nearly degenerate, with their masses separated by their tree level decay width. This scenario led to resonant leptogenesis (or TeV scale leptogenesis) for the production of observed baryon asymmetry in the Universe from the out of equilibrium decays of RH neutrinos. We generated the observed baryon asymmetry for three different values of RH neutrino masses namely $M_{N_1} = 1600$ GeV, 1800 GeV and 2000 GeV, respectively, where required values of CP asymmetry parameter parameter (ε_1) were 4.4×10^{-4}, 2.25×10^{-4} and 1.8×10^{-4}, respectively. These values of M_{N_1} and ϵ_1 were also seen to be allowed by the neutrino oscillation data.

Lastly, we studied the DM phenomenology by considering a FIMP type DM candidate ϕ_{DM}. We took into account all the production modes of ϕ_{DM} (both before and after EWSB) arising from the annihilations and decays of SM as well as BSM particles. We found that the production of ϕ_{DM} mostly occurred from the decays of h_1 and h_2, however there are some regions in the model parameter space where annihilations from W^+W^-, ZZ, h_1h_1 can contribute dominant to the relic density of ϕ_{DM}. We also found that for a FIMP candidate ϕ_{DM} the observed DM relic density ($0.1172 \leq \Omega_{h^2} \leq 0.1226$) is generated via the freeze-in mechanism where the scalar portal couplings of ϕ_{DM} are bounded by following limits $\lambda_{Dh} \lesssim 10^{-11}$ and $\lambda_{DH} \lesssim 10^{-12}$ for 10 GeV $\leq M_{DM} \leq 100$ GeV. Hence, ϕ_{DM} can easily evade all the constrains coming from any terrestrial DM direct detection experiment.

In conclusion, our spontaneously broken local $\mathrm{U(1)_{B-L}}$ extension of the SM with three additional RH and two additional scalars can explain the three main evidences for physics beyond the SM, *viz.*, small neutrino masses, matter-antimatter asymmetry of the Universe and dark matter. Tiny neutrino masses and all mixing angles can be obtained via Type I seesaw mechanism where we chose a certain pattern for the real and complex Yukawa couplings. The model gave a definite prediction for the CP violating phase to be measured in the next generation long baseline experiments. The dark matter candidate is the scalar neutral under both the SM gauge group and $\mathrm{U(1)_{B-L}}$ gauge group and is made stable by an additional $\mathbb{Z}_2$. This scalar DM can easily be taken

as a FIMP candidate. The masses of the RH neutrinos are taken in the TeV regime and two of them taken as nearly degenerate, which allows for richer collider phenomenology and resonant leptogenesis where using the latter process, the observed baryon asymmetry of the Universe can be easily obtained.

V. ACKNOWLEDGEMENT

SK and AB also acknowledge the HRI cluster computing facility (http://cluster.hri.res.in). The authors would also like to thank the Department of Atomic Energy (DAE) Neutrino Project under the XII plan of Harish-Chandra Research Institute. This project has received funding from the European Union's Horizon 2020 research and innovation programme InvisiblesPlus RISE under the Marie Sklodowska-Curie grant agreement No 690575. This project has received funding from the European Union's Horizon 2020 research and innovation programme Elusives ITN under the Marie Sklodowska- Curie grant agreement No 674896.

Appendix A: Expression for the Majorana mass matrix of light neutrinos

Here we have given the expression of all the elements of the light neutrino mass matrix m_ν in terms of the Yukawa couplings and the RH neutrino masses.

$$
\begin{aligned}
(m_\nu)_{11} &= -\frac{y_{ee}^2}{M_{N_1}} - \frac{y_{e\mu}^2}{M_{N_2}} - \frac{y_{e\tau}^2}{M_{N_3}}, \\
(m_\nu)_{12} &= -\frac{y_{e\mu}\, y_{\mu\mu}}{M_{N_2}} - \frac{y_{e\tau}\, y_{\mu\tau}}{M_{N_3}} - \frac{y_{ee}\, y_{\mu e}}{M_{N_1}} - i\,\frac{y_{ee}\,\tilde{y}_{\mu e}}{M_{N_1}}, \\
(m_\nu)_{13} &= -\frac{y_{e\tau}\, y_{\tau\tau}}{M_{N_3}} - \frac{y_{ee}\, y_{\tau e}}{M_{N_1}} - \frac{y_{e\mu}\, y_{\tau\mu}}{M_{N_2}} - i\left(\frac{y_{ee}\,\tilde{y}_{\tau e}}{M_{N_1}} + \frac{y_{e\mu}\,\tilde{y}_{\tau\mu}}{M_{N_2}}\right), \\
(m_\nu)_{21} &= (m_\nu)_{12}, \\
(m_\nu)_{22} &= -\frac{y_{\mu\mu}^2}{M_{N_2}} - \frac{y_{\mu\tau}^2}{M_{N_3}} - \frac{y_{\mu e}^2}{M_{N_1}} + \frac{\tilde{y}_{\mu e}^2}{M_{N_1}} - i\,\frac{2\, y_{\mu e}\,\tilde{y}_{\mu e}}{M_{N_1}}, \\
(m_\nu)_{23} &= -\frac{y_{\mu\tau}\, y_{\tau\tau}}{M_{N_3}} - \frac{y_{\mu e}\, y_{\tau e}}{M_{N_1}} - \frac{y_{\mu\mu}\, y_{\tau\mu}}{M_{N_2}} + \frac{\tilde{y}_{\mu e}\,\tilde{y}_{\tau e}}{M_{N_1}} - i\left(\frac{y_{\tau e}\,\tilde{y}_{\mu e}}{M_{N_1}} + \frac{y_{\mu e}\,\tilde{y}_{\tau e}}{M_{N_1}} + \frac{y_{\mu\mu}\,\tilde{y}_{\tau\mu}}{M_{N_2}}\right), \\
(m_\nu)_{31} &= (m_\nu)_{13}, \\
(m_\nu)_{32} &= (m_\nu)_{23}, \\
(m_\nu)_{33} &= -\frac{y_{\tau\tau}^2}{M_{N_3}} - \frac{y_{\tau e}^2}{M_{N_1}} - \frac{y_{\tau\mu}^2}{M_{N_2}} + \frac{\tilde{y}_{\tau e}^2}{M_{N_1}} + \frac{\tilde{y}_{\tau\mu}^2}{M_{N_2}} - i\,2\left(\frac{y_{\tau e}\,\tilde{y}_{\tau e}}{M_{N_1}} + \frac{y_{\tau\mu}\,\tilde{y}_{\tau\mu}}{M_{N_2}}\right),
\end{aligned}
\tag{A1}
$$

$$
m_\nu = \begin{pmatrix} (m_\nu)_{11} & (m_\nu)_{12} & (m_\nu)_{13} \\ (m_\nu)_{21} & (m_\nu)_{22} & (m_\nu)_{23} \\ (m_\nu)_{31} & (m_\nu)_{32} & (m_\nu)_{33} \end{pmatrix}. \tag{A2}
$$

Appendix B: Neutrino less double β decay parameter $m_{\beta\beta}$

Since the light neutrino mass matrix is Majorana in nature, it is a complex symmetric matrix. A complex symmetric matrix m_ν can be diagonalised by a Unitary matrix $U_{\rm PMNS}$ (defined in Eq. (20)) in the following way,

$$
\begin{aligned}
m_{\rm diag} &= U_{\rm PMNS}^\dagger\, m_\nu\, U_{\rm PMNS}^*, \\
\Rightarrow m_\nu &= U_{\rm PMNS}\, m_{\rm diag}\, U_{\rm PMNS}^T.
\end{aligned}
$$

Now equating the $(i,\, j)^{\rm th}$ element from both sides of the above equation, we get

$$
(m_\nu)_{ij} = (U_{\rm PMNS})_{ik}\, (m_{\rm diag})_{kk'}\, (U_{\rm PMNS}^T)_{k'j}.
$$

Since $m_{\rm dia}$ is a diagonal matrix, we can further simplify $(m_\nu)_{ij}$ by using $m_{\rm diag} = m_k\,\delta_{kk'}$, where m_k is the mass of $k^{\rm th}$ light neutrino. Therefore $(m_\nu)_{ij}$ takes the following form

$$(m_\nu)_{ij} = \sum_{k=1}^{3} m_k\,(U_{\rm PMNS})_{ik}\,(U_{\rm PMNS})_{jk}\,.$$

Above equation expresses the elements of light neutrino mass matrix (Eq. (A1)) in terms of the light neutrino masses, the intergenerational mixing angles and the phases. Taking $i = j = 1$, we get the expression of the (1,1) element of m_ν i.e.

$$(m_\nu)_{11} = \sum_{k=1}^{3} m_k\,(U_{\rm PMNS})^2_{1\,k},$$

which is related to the important parameter $m_{\beta\beta}$ of the neutrino less double β decay [62] as,

$$m_{\beta\beta} = \left|\sum_{k=1}^{3} m_k\,(U_{\rm PMNS})^2_{1\,k}\right| = |(m_\nu)_{11}|\,. \tag{B1}$$

Appendix C: Expressions of decay widths of h_2, h_1 and Z_{BL}

In the present work, we have considered the effect of electroweak symmetry breaking on dark matter production. After EWSB SM particles become massive and affect DM production, while before EWSB those particles have no effect. To take this effect into account we have defined an extra constant C_{ASB}. In all the equations, the value of the constant $C_{ASB} = 0$ before the EWSB and this is equal to unity i.e. $C_{ASB} = 1$ after the EWSB. Also before the EWSB, there is no mixing between the SM and BSM Higgs bosons, i.e. $\alpha = 0$. The two vertices which are common to all Higgs mediated diagrams are as follows,

$$\begin{aligned} g_{h_1\phi_{DM}\phi_{DM}} &= -2\,(v\lambda_{Dh}\cos\alpha + v_{BL}\lambda_{DH}\sin\alpha)\,, \\ g_{h_2\phi_{DM}\phi_{DM}} &= 2\,(v\lambda_{Dh}\sin\alpha - v_{BL}\lambda_{DH}\cos\alpha)\,. \end{aligned} \tag{C1}$$

Total decay width of h_2:

- $h_2 \to VV$ $(V = W^\pm, Z)$:

$$\begin{aligned} g_{h_2VV} &= -\frac{2M_V^2}{v}\,\sin\alpha\,, \\ \Gamma(h_2 \to VV) &= \frac{C_{ASB}\,M_{h_2}^3\,g_{h_2VV}^2}{64\,\pi M_V^4\,S_V}\sqrt{1-\frac{4M_V^2}{M_{h_2}^2}}\,\left(1-\frac{4M_V^2}{M_{h_2}^2}+\frac{12M_V^4}{M_{h_2}^4}\right)\,, \end{aligned} \tag{C2}$$

where $S_V = 2\,(1)$ for $ZZ\,(W^+W^-)$ final state.

- $\underline{h_2 \to h_1\, h_1}$:

$$\Gamma(h_2 \to h_1 h_1) = \frac{g^2_{h_1 h_1 h_2}}{32\,\pi\, M_{h_2}} \sqrt{1 - \frac{4M^2_{h_1}}{M^2_{h_2}}}\,. \tag{C3}$$

- $\underline{h_2 \to \phi_{DM}\ \phi_{DM}}$:

$$\Gamma(h_2 \to \phi_{DM}\phi_{DM}) \;=\; \frac{g^2_{h_2\phi_{DM}\phi_{DM}}}{32\,\pi\, M_{h_2}} \sqrt{1 - \frac{4M^2_{DM}}{M^2_{h_2}}}\,, \tag{C4}$$

- $\underline{h_2 \to f\bar{f}}$:

$$\begin{aligned} g_{h_2 ff} \;&=\; \frac{M_f}{v}\,\sin\alpha\,, \\ \Gamma(h_2 \to \mathrm{f}\,\bar{\mathrm{f}}) \;&=\; \frac{C_{ASB}\ n_c\, M_{h_2}\, g_{h_2 ff}}{8\pi} \left(1 - \frac{4M^2_f}{M^2_{h_2}}\right)^{\frac{3}{2}}\,, \end{aligned} \tag{C5}$$

n_c is the color charge, for leptons it is 1 and for quarks it is 3.

Total decay width of the extra Higgs h_2 in the present case is,

$$\begin{aligned} \Gamma_{h_2} = \sum_{V=W,Z} \Gamma(h_2 \to VV) + \Gamma(h_2 \to h_1 h_1) + \Gamma(h_2 \to \phi_{DM}\phi_{DM}) \\ + \sum_f \Gamma(h_2 \to f\,\bar{f})\,. \end{aligned} \tag{C6}$$

$\underline{\text{Decay width of } h_1}$:

$$\Gamma(h_1 \to \phi_{DM}\phi_{DM}) \;=\; \frac{C_{ASB}\ g^2_{h_1\phi_{DM}\phi_{DM}}}{32\,\pi\, M_{h_1}} \sqrt{1 - \frac{4M^2_{DM}}{M^2_{h_1}}}\,, \tag{C7}$$

Total decay width of SM-like Higgs boson is,

$$\Gamma_{h_1} = \cos^2\alpha\,\Gamma_{SM} + \Gamma(h_1 \to \phi_{DM}\phi_{DM})\ , \tag{C8}$$

where Γ_{SM} is the total decay width of SM Higgs boson.

Decay width of Z_{BL}:

$$\begin{aligned}
\Gamma(Z_{BL} \to f\bar{f}) &= \frac{M_{Z_{BL}}}{12\pi} n_c (q_f\, g_{BL})^2 \left(1 + \frac{2M_f^2}{M_{Z_{BL}}^2}\right) \sqrt{1 - \frac{4M_f^2}{M_{Z_{BL}}^2}}\,, \\
\Gamma(Z_{BL} \to \nu_x \bar{\nu_x}) &= \frac{M_{Z_{BL}}}{24\pi} g_{BL}^2 \left(1 - \frac{4M_{\nu_x}^2}{M_{Z_{BL}}^2}\right)^{\frac{3}{2}}\,, \\
\Gamma(Z_{BL} \to N_x \bar{N}_x) &= \frac{M_{Z_{BL}}}{24\pi} g_{BL}^2 \left(1 - \frac{4M_{N_x}^2}{M_{Z_{BL}}^2}\right)^{\frac{3}{2}}\,.
\end{aligned}$$

Total decay width of the extra neutral gauge boson Z_{BL} is,

$$\Gamma_{Z_{BL}} = \sum_f \Gamma(Z_{BL} \to f\bar{f}) + \Gamma(Z_{BL} \to \nu_x \bar{\nu_x}) + \Gamma(Z_{BL} \to N_x \bar{N}_x)\,. \tag{C9}$$

Appendix D: Analytical Expression of relevant Cross sections

Here we will give the expressions of cross sections for all relevant processes which take part in the FIMP DM production.

- $h_1\, h_1 \to \phi_{DM}\, \phi_{DM}$:

$$\begin{aligned}
g_{h_1 h_1 h_1} &= -3\,[2\,v\lambda_h \cos^3\alpha + 2\,v_{BL}\,\lambda_H \sin^3\alpha + \lambda_{hH} \sin\alpha\, \cos\alpha\, (v \sin\alpha + v_{BL} \cos\alpha)], \\
g_{h_1 h_1 h_2} &= [6\,v\lambda_h \cos^2\alpha \sin\alpha - 6\,v_{BL}\lambda_H \sin^2\alpha\, \cos\alpha - (2 - 3\,\sin^2\alpha)\, v\, \lambda_{hH}\, \sin\alpha \\
&\quad -(1 - 3\sin^2\alpha) v_{BL}\, \lambda_{hH} \cos\alpha]\,, \qquad \text{(D1)} \\
g_{h_1 h_1 \phi_{DM}\phi_{DM}} &= -2\,(\lambda_{Dh} \cos^2\alpha + \lambda_{DH} \sin^2\alpha)\,, \\
M_{h_1 h_1} &= \left(\frac{C_{ASB}\, g_{h_1 h_1 h_1}\, g_{h_1 \phi_{DM}\phi_{DM}}}{(s - M_{h_1}^2) + iM_{h_1}\Gamma_{h_1}} + \frac{g_{h_1 h_1 h_2}\, g_{h_2 \phi_{DM}\phi_{DM}}}{(s - M_{h_2}^2) + iM_{h_2}\Gamma_{h_2}}\right) - g_{h_1 h_1 \phi_{DM}\phi_{DM}}, \\
\sigma_{h_1 h_1 \to \phi_{DM}\phi_{DM}} &= \frac{1}{32\pi s} \sqrt{\frac{s - 4M_{DM}^2}{s - 4M_{h_1}^2}}\; |M_{h_1 h_1}|^2\,. \qquad \text{(D2)}
\end{aligned}$$

- $\underline{h_2\, h_2 \to \phi_{DM}\, \phi_{DM}}$:

$$
\begin{aligned}
g_{h_2h_2h_2} &= 3\,[2\,v\lambda_h \sin^3\alpha - 2\,v_{BL}\lambda_H \cos^3\alpha + \lambda_{hH} \sin\alpha\cos\alpha\,(v\cos\alpha - v_{BL}\sin\alpha)],\\
g_{h_2h_2h_1} &= -[6\,v\lambda_h \sin^2\alpha\cos\alpha + 6\,v_{BL}\lambda_H \cos^2\alpha\sin\alpha - (2-3\,\sin^2\alpha)v_{BL}\lambda_{hH}\sin\alpha\\
&\quad +(1-3\sin^2\alpha)v\lambda_{hH}\cos\alpha]\,,\\
g_{h_2h_2\phi_{DM}\phi_{DM}} &= -2\,(\lambda_{Dh}\sin^2\alpha + \lambda_{DH}\cos^2\alpha)\,,\\
M_{h_2h_2} &= \left(C_{ASB}\;\frac{g_{h_2h_2h_1}\;g_{h_1\phi_{DM}\phi_{DM}}}{(s-M_{h_1}^2)+iM_{h_1}\Gamma_{h_1}} + \frac{g_{h_2h_2h_2}\;g_{h_2\phi_{DM}\phi_{DM}}}{(s-M_{h_2}^2)+iM_{h_2}\Gamma_{h_2}}\right) - g_{h_2h_2\phi_{DM}\phi_{DM}},\\
\sigma_{h_2h_2\to\phi_{DM}\phi_{DM}} &= \frac{1}{32\pi s}\,\sqrt{\frac{s-4M_{DM}^2}{s-4M_{h_2}^2}}\;|M_{h_2h_2}|^2\,.
\end{aligned}
\tag{D3}
$$

- $\underline{h_1\, h_2 \to \phi_{DM}\, \phi_{DM}}$:

$$
\begin{aligned}
g_{h_1h_1h_2} &= [6\,v\lambda_h\cos^2\alpha\,\sin\alpha - 6\,v_{BL}\,\lambda_H\sin^2\alpha\,\cos\alpha - (2-3\,\sin^2\alpha)\,v\,\lambda_{hH}\sin\alpha\\
&\quad -(1-3\sin^2\alpha)v_{BL}\,\lambda_{hH}\cos\alpha]\\
g_{h_2h_2h_1} &= -[6\,v\lambda_h\sin^2\alpha\,\cos\alpha + 6\,v_{BL}\lambda_H\cos^2\alpha\sin\alpha - (2-3\,\sin^2\alpha)\,v_{BL}\,\lambda_{hH}\sin\alpha\\
&\quad +(1-3\sin^2\alpha)v\lambda_{hH}\cos\alpha]\,,\\
g_{h_1h_2\phi_{DM}\phi_{DM}} &= 2\,\sin\alpha\cos\alpha(\lambda_{Dh}-\lambda_{DH})\,,\\
M_{h_1h_2} &= -C_{ASB}\left(g_{h_1h_2\phi_{DM}\phi_{DM}} - \frac{g_{h_2h_2h_1}\;g_{h_2\phi_{DM}\phi_{DM}}}{(s-M_{h_2}^2)+iM_{h_2}\Gamma_{h_2}}\right) + \frac{g_{h_1h_1h_2}\;g_{h_1\phi_{DM}\phi_{DM}}}{(s-M_{h_1}^2)+iM_{h_1}\Gamma_{h_1}},\\
\sigma_{h_1h_2\to\phi_{DM}\phi_{DM}} &= \frac{1}{32\pi s}\,\sqrt{\frac{s(s-4M_{DM}^2)}{(s-(M_{h_1}+M_{h_2})^2)(s-(M_{h_2}-M_{h_1})^2)}}\;|M_{h_1h_2}|^2\,.
\end{aligned}
\tag{D4}
$$

- $\underline{W^+\,W^- \to \phi_{DM}\, \phi_{DM}}$:

$$
\begin{aligned}
g_{h_1WW} &= \frac{2M_W^2\cos\alpha}{v}\,,\\
g_{h_2WW} &= -\frac{2M_W^2\sin\alpha}{v},\\
A_{WW} &= C_{ASB}\left(\frac{g_{h_1WW}\;g_{h_1\phi_{DM}\phi_{DM}}}{(s-M_{h_1}^2)+iM_{h_1}\Gamma_{h_1}} + \frac{g_{h_2WW}\,g_{h_2\phi_{DM}\phi_{DM}}}{(s-M_{h_2}^2)+iM_{h_2}\Gamma_{h_2}}\right),\\
M_{WW} &= \frac{2}{9}\left(1+\frac{(s-2M_W^2)^2}{8M_W^4}\right)\,A_{WW},\\
\sigma_{WW\to\phi_{DM}\phi_{DM}} &= \frac{1}{32\pi s}\,\sqrt{\frac{s-4M_{DM}^2}{s-4M_W^2}}\;|M_{WW}|^2\,.
\end{aligned}
\tag{D5}
$$

- $\underline{Z\,Z \to \phi_{DM}\,\phi_{DM}}$:

$$\begin{aligned}
g_{h_1 ZZ} &= \frac{2M_Z^2 \cos\alpha}{v}\,, \\
g_{h_2 ZZ} &= -\frac{2M_Z^2 \sin\alpha}{v}, \\
A_{ZZ} &= C_{ASB}\left(\frac{g_{h_1 ZZ}\, g_{h_1\phi_{DM}\phi_{DM}}}{(s-M_{h_1}^2)+iM_{h_1}\Gamma_{h_1}} + \frac{g_{h_2 ZZ}\, g_{h_2\phi_{DM}\phi_{DM}}}{(s-M_{h_2}^2)+iM_{h_2}\Gamma_{h_2}}\right), \\
M_{ZZ} &= \frac{2}{9}\,\left(1+\frac{(s-2M_Z^2)^2}{8M_Z^4}\right)\,A_{ZZ}, \\
\sigma_{ZZ\to\phi_{DM}\phi_{DM}} &= \frac{1}{32\pi s}\,\sqrt{\frac{s-4M_{DM}^2}{s-4M_Z^2}}\;\,|M_{ZZ}|^2\,.
\end{aligned} \tag{D6}$$

- $\underline{t\bar{t}\;\to \phi_{DM}\,\phi_{DM}}$:

$$\begin{aligned}
g_{h_1 tt} &= -\frac{M_t}{v}\cos\alpha\,, \\
g_{h_2 tt} &= \frac{M_t}{v}\sin\alpha\,, \\
M_{tt} &= C_{ASB}\left(\frac{g_{h_1 tt}\;g_{h_1\phi_{DM}\phi_{DM}}}{(s-M_{h_1}^2)+iM_{h_1}\Gamma_{h_1}} + \frac{g_{h_2 tt}\;g_{h_2\phi_{DM}\phi_{DM}}}{(s-M_{h_2}^2)+iM_{h_2}\Gamma_{h_2}}\right), \\
\sigma_{t\bar{t}\to\phi_{DM}\phi_{DM}} &= \frac{1}{64\pi s\, n_c}\;(s-4M_t^2)\,\sqrt{\frac{s-4M_{DM}^2}{s-4M_t^2}}\;\,|M_{tt}|^2\,,
\end{aligned} \tag{D7}$$

- $\underline{N_i\,N_i \to \phi_{DM}\,\phi_{DM}\;\;(i=1,\,2,\,3)}$:

$$\begin{aligned}
g_{h_1 N_i N_i} &= \frac{y_{N_i}\sin\alpha}{\sqrt{2}}\,, \\
g_{h_2 N_i N_i} &= \frac{y_{N_i}\cos\alpha}{\sqrt{2}}\,, \\
M_{N_i N_i} &= \frac{C_{ASB}\;g_{h_1 N_i N_i}\;g_{h_1\phi_{DM}\phi_{DM}}}{(s-M_{h_1}^2)+iM_{h_1}\Gamma_{h_1}} + \frac{g_{h_2 N_i N_i}\;g_{h_2\phi_{DM}\phi_{DM}}}{(s-M_{h_2}^2)+iM_{h_2}\Gamma_{h_2}}\,, \\
\sigma_{N_i N_i\to\phi_{DM}\phi_{DM}} &= \frac{(s-4\,M_{N_j}^2)}{64\pi s}\,\sqrt{\frac{(s-4M_{DM}^2)}{(s-4M_{N_i}^2)}}\;\,|M_{N_i N_i}|^2\,.
\end{aligned} \tag{D8}$$

---

[1] Y. Fukuda *et al.* [Super-Kamiokande Collaboration], "*Evidence for oscillation of atmospheric neutrinos*", Phys. Rev. Lett. **81**, 1562 (1998) [hep-ex/9807003].

[2] Q. R. Ahmad *et al.* [SNO Collaboration], "*Direct evidence for neutrino flavor transformation from neutral current interactions in the Sudbury Neutrino Observatory*", Phys. Rev. Lett. **89**, 011301 (2002) [nucl-ex/0204008].

[3] K. Eguchi *et al.* [KamLAND Collaboration], "*First results from KamLAND: Evidence for reactor anti-neutrino disappearance*", Phys. Rev. Lett. **90**, 021802 (2003) [hep-ex/0212021].

[4] F. P. An *et al.* [Daya Bay Collaboration], "*Measurement of the Reactor Antineutrino Flux and Spectrum at Daya Bay*", Phys. Rev. Lett. **116**, no. 6, 061801 (2016) [arXiv:1508.04233 [hep-ex]].

[5] J. H. Choi *et al.* [RENO Collaboration], "*Observation of Energy and Baseline Dependent Reactor Antineutrino Disappearance in the RENO Experiment*", Phys. Rev. Lett. **116**, no. 21, 211801 (2016) [arXiv:1511.05849 [hep-ex]].

[6] Y. Abe *et al.* [Double Chooz Collaboration], "*Improved measurements of the neutrino mixing angle θ_{13} with the Double Chooz detector*", JHEP **1410**, 086 (2014) Erratum: [JHEP **1502**, 074 (2015)] [arXiv:1406.7763 [hep-ex]].

[7] K. Abe *et al.* [T2K Collaboration], "*Measurements of neutrino oscillation in appearance and disappearance channels by the T2K experiment with 6.6×10^{20} protons on target*", Phys. Rev. D **91**, no. 7, 072010 (2015) [arXiv:1502.01550 [hep-ex]].

[8] M. Ravonel Salzgeber [T2K Collaboration], "*Anti-neutrino oscillations with T2K*", arXiv:1508.06153 [hep-ex].

[9] P. Adamson *et al.* [NOvA Collaboration], "*First measurement of electron neutrino appearance in NOvA*", Phys. Rev. Lett. **116**, no. 15, 151806 (2016) [arXiv:1601.05022 [hep-ex]].

[10] P. Adamson *et al.* [NOvA Collaboration], "*First measurement of muon-neutrino disappearance in NOvA*", Phys. Rev. D **93**, no. 5, 051104 (2016) [arXiv:1601.05037 [hep-ex]].

[11] Talk on "*Recent results from T2K and Future Prospects*", https://indico.cern.ch/event/432527/contributions/2143636/

[12] A. Gando *et al.* [KamLAND-Zen Collaboration], "*Search for Majorana Neutrinos near the Inverted Mass Hierarchy Region with KamLAND-Zen*", Phys. Rev. Lett. **117**, no. 8, 082503 (2016) Addendum: [Phys. Rev. Lett. **117**, no. 10, 109903 (2016)] [arXiv:1605.02889 [hep-ex]].

[13] A. Gando *et al.* [KamLAND-Zen Collaboration], "*Limit on Neutrinoless $\beta\beta$ Decay of ^{136}Xe from the First Phase of KamLAND-Zen and Comparison with the Positive Claim in ^{76}Ge*", Phys. Rev. Lett. **110**, no. 6, 062502 (2013) [arXiv:1211.3863 [hep-ex]].

[14] K. Asakura *et al.* [KamLAND-Zen Collaboration], "*Results from KamLAND-Zen*", AIP Conf. Proc. **1666**, 170003 (2015) [arXiv:1409.0077 [physics.ins-det]].

[15] J. B. Albert *et al.* [EXO-200 Collaboration], "*Search for Majorana neutrinos with the first two years of EXO-200 data*", Nature **510**, 229 (2014) [arXiv:1402.6956 [nucl-ex]].

[16] M. Agostini [GERDA Collaboration], Conference Presen- tation, Neutrino 2016

[17] M. Agostini *et al.* [GERDA Collaboration], "*Results on Neutrinoless Double-β Decay of ^{76}Ge*

from Phase I of the GERDA Experiment", Phys. Rev. Lett. **111**, no. 12, 122503 (2013) doi:10.1103/PhysRevLett.111.122503 [arXiv:1307.4720 [nucl-ex]].

[18] Y. Sofue and V. Rubin, "*Rotation curves of spiral galaxies*", Ann. Rev. Astron. Astrophys. **39**, 137 (2001) [astro-ph/0010594].

[19]

[19] M. Bartelmann and P. Schneider, "*Weak gravitational lensing*", Phys. Rept. **340**, 291 (2001) [astro-ph/9912508].

[20] D. Clowe, A. Gonzalez and M. Markevitch, "*Weak lensing mass reconstruction of the interacting cluster 1E0657-558: Direct evidence for the existence of dark matter*", Astrophys. J. **604**, 596 (2004) [astro-ph/0312273].

[21] D. Harvey, R. Massey, T. Kitching, A. Taylor and E. Tittley, "*The non-gravitational interactions of dark matter in colliding galaxy clusters*", Science **347**, 1462 (2015) [arXiv:1503.07675 [astro-ph.CO]].

[22] A. Biviano, P. Katgert, A. Mazure, M. Moles, R. denHartog, J. Perea and P. Focardi, "*The eso nearby abell cluster survey. 3. Distribution and kinematics of emission-line galaxies*", Astron. Astrophys. **321**, 84 (1997) [astro-ph/9610168].

[23] D. Harvey, R. Massey, T. Kitching, A. Taylor and E. Tittley, "*The non-gravitational interactions of dark matter in colliding galaxy clusters*", Science **347** (2015) 1462 [arXiv:1503.07675 [astro-ph.CO]].

[24] G. Hinshaw *et al.* [WMAP Collaboration], "*Nine-Year Wilkinson Microwave Anisotropy Probe (WMAP) Observations: Cosmological Parameter Results*", Astrophys. J. Suppl. **208**, 19 (2013) [arXiv:1212.5226 [astro-ph.CO]].

[25] P. A. R. Ade *et al.* [Planck Collaboration], "*Planck 2015 results. XIII. Cosmological parameters*", arXiv:1502.01589 [astro-ph.CO].

[26] E. Aprile [XENON1T Collaboration], "*The XENON1T Dark Matter Search Experiment*", Springer Proc. Phys. **148**, 93 (2013) [arXiv:1206.6288 [astro-ph.IM]].

[27] D. S. Akerib *et al.* [LUX Collaboration], "*Improved Limits on Scattering of Weakly Interacting Massive Particles from Reanalysis of 2013 LUX Data*", Phys. Rev. Lett. **116**, no. 16, 161301 (2016) [arXiv:1512.03506 [astro-ph.CO]].

[28] Z. Ahmed *et al.* [CDMS-II Collaboration], "*Results from a Low-Energy Analysis of the CDMS II Germanium Data*", Phys. Rev. Lett. **106**, 131302 (2011) [arXiv:1011.2482 [astro-ph.CO]].

[29] G. Jungman, M. Kamionkowski and K. Griest, "Supersymmetric dark matter", Phys. Rept. **267**, 195 (1996) [hep-ph/9506380].

[30] N. Arkani-Hamed, D. P. Finkbeiner, T. R. Slatyer and N. Weiner, "*A Theory of Dark Matter*", Phys. Rev. D **79**, 015014 (2009) [arXiv:0810.0713 [hep-ph]].

[31] L. J. Hall, K. Jedamzik, J. March-Russell and S. M. West, "*Freeze-In Production of FIMP Dark Matter*" JHEP **1003**, 080 (2010) [arXiv:0911.1120 [hep-ph]].

[32] C. E. Yaguna, "*The Singlet Scalar as FIMP Dark Matter*" JHEP **1108**, 060 (2011) [arXiv:1105.1654 [hep-ph]].

[33] E. Molinaro, C. E. Yaguna and O. Zapata, "*FIMP realization of the scotogenic model*" JCAP **1407**, 015 (2014) [arXiv:1405.1259 [hep-ph]].

[34] A. Biswas, D. Majumdar and P. Roy, "*Nonthermal two component dark matter model for Fermi-LAT γ-ray excess and* 3.55 *keV X-ray line*" JHEP **1504**, 065 (2015) [arXiv:1501.02666 [hep-ph]].

[35] A. Merle and M. Totzauer, "*keV Sterile Neutrino Dark Matter from Singlet Scalar Decays: Basic Concepts and Subtle Features*" JCAP **1506**, 011 (2015) [arXiv:1502.01011 [hep-ph]].

[36] B. Shakya, "*Sterile Neutrino Dark Matter from Freeze-In*" Mod. Phys. Lett. A **31**, no. 06, 1630005 (2016) [arXiv:1512.02751 [hep-ph]].

[37] A. Biswas and A. Gupta, "*Freeze-in Production of Sterile Neutrino Dark Matter in U(1)$_{\rm B-L}$ Model*" JCAP **1609**, no. 09, 044 (2016) [arXiv:1607.01469 [hep-ph]].

[38] J. König, A. Merle and M. Totzauer, "*keV Sterile Neutrino Dark Matter from Singlet Scalar Decays: The Most General Case*" JCAP **1611**, no. 11, 038 (2016) [arXiv:1609.01289 [hep-ph]].

[39] A. Biswas and A. Gupta, "*Calculation of Momentum Distribution Function of a Non-thermal Fermionic Dark Matter*", JCAP03(2017)033 [arXiv:1612.02793 [hep-ph]].

[40] A. Biswas, S. Choubey and S. Khan, "*FIMP and Muon ($g-2$) in a $U(1)_{L_\mu - L_\tau}$ Model*", JHEP **1702**, 123 (2017) [arXiv:1612.03067 [hep-ph]].

[41] C. Patrignani *et al.* [Particle Data Group], "*Review of Particle Physics*", Chin. Phys. C **40**, no. 10, 100001 (2016).

[42] A. D. Sakharov, "*Violation of CP Invariance, c Asymmetry, and Baryon Asymmetry of the Universe*", Pisma Zh. Eksp. Teor. Fiz. **5**, 32 (1967) [JETP Lett. **5**, 24 (1967)] [Sov. Phys. Usp. **34**, 392 (1991)] [Usp. Fiz. Nauk **161**, 61 (1991)].

[43] N. S. Manton, "*Topology in the Weinberg-Salam Theory*", Phys. Rev. D **28**, 2019 (1983).

[44] F. R. Klinkhamer and N. S. Manton, "*A Saddle Point Solution in the Weinberg-Salam Theory*", Phys. Rev. D **30**, 2212 (1984).

[45] V. A. Kuzmin, V. A. Rubakov and M. E. Shaposhnikov, "*On the Anomalous Electroweak Baryon Number Nonconservation in the Early Universe*", Phys. Lett. **155B**, 36 (1985). doi:10.1016/0370-2693(85)91028-7

[46] S. Y. Khlebnikov and M. E. Shaposhnikov, "*The Statistical Theory of Anomalous Fermion Number Nonconservation*", Nucl. Phys. B **308**, 885 (1988).

[47] G. Arcadi and L. Covi, "*Minimal Decaying Dark Matter and the LHC*", JCAP **1308**, 005 (2013) [arXiv:1305.6587 [hep-ph]].

[48] M. Plumacher, "*Baryogenesis and lepton number violation*", Z. Phys. C **74**, 549 (1997), [hep-ph/9604229].

[49] W. Buchmuller, P. Di Bari and M. Plumacher, "*Cosmic microwave background, matter - antimatter*

asymmetry and neutrino masses" Nucl. Phys. B **643**, 367 (2002) Erratum: [Nucl. Phys. B **793**, 362 (2008)] [hep-ph/0205349].

[50] S. Iso, N. Okada and Y. Orikasa, "*Resonant Leptogenesis in the Minimal B-L Extended Standard Model at TeV*", Phys. Rev. D **83**, 093011 (2011), [arXiv:1011.4769 [hep-ph]].

[51] M. Flanz, E. A. Paschos, U. Sarkar and J. Weiss, "*Baryogenesis through mixing of heavy Majorana neutrinos*", Phys. Lett. B **389**, 693 (1996), [hep-ph/9607310].

[52] A. Pilaftsis, "*CP violation and baryogenesis due to heavy Majorana neutrinos*", Phys. Rev. D **56**, 5431 (1997), [hep-ph/9707235].

[53] A. Pilaftsis and T. E. J. Underwood, "*Resonant leptogenesis*", Nucl. Phys. B **692**, 303 (2004), [hep-ph/0309342].

[54] A. Biswas, S. Choubey and S. Khan, "*Galactic gamma ray excess and dark matter phenomenology in a $U(1)_{B-L}$ model*", JHEP **1608**, 114 (2016), [arXiv:1604.06566 [hep-ph]].

[55] N. Chakrabarty, D. K. Ghosh, B. Mukhopadhyaya and I. Saha, "*Dark matter, neutrino masses and high scale validity of an inert Higgs doublet model*", Phys. Rev. D **92**, no. 1, 015002 (2015) [arXiv:1501.03700 [hep-ph]].

[56] C. Jarlskog, "*Commutator of the Quark Mass Matrices in the Standard Electroweak Model and a Measure of Maximal CP Violation*", Phys. Rev. Lett. **55**, 1039 (1985).

[57] F. Capozzi, E. Lisi, A. Marrone, D. Montanino and A. Palazzo, "*Neutrino masses and mixings: Status of known and unknown 3ν parameters*", Nucl. Phys. B **908**, 218 (2016), [arXiv:1601.07777 [hep-ph]].

[58] S. L. Adler, "*Axial vector vertex in spinor electrodynamics*", Phys. Rev. **177**, 2426 (1969).

[59] W. A. Bardeen, "*Anomalous Ward identities in spinor field theories*", Phys. Rev. **184**, 1848 (1969).

[60] R. Delbourgo and A. Salam, "*The gravitational correction to pcac*", Phys. Lett. B **40**, 381 (1972).

[61] T. Eguchi and P. G. O. Freund, "*Quantum Gravity and World Topology*", Phys. Rev. Lett. **37**, 1251 (1976).

[62] S. Dell'Oro, S. Marcocci, M. Viel and F. Vissani, "*Neutrinoless double beta decay: 2015 review*", Adv. High Energy Phys. **2016**, 2162659 (2016) [arXiv:1601.07512 [hep-ph]].

[63] J. Edsjo and P. Gondolo, "*Neutralino relic density including coannihilations*", Phys. Rev. D **56**, 1879 (1997) [hep-ph/9704361].

[64] P. Gondolo and G. Gelmini, "*Cosmic abundances of stable particles: Improved analysis*" Nucl. Phys. B **360**, 145 (1991).

[65] A. Biswas and D. Majumdar, "*The Real Gauge Singlet Scalar Extension of Standard Model: A Possible Candidate of Cold Dark Matter*", Pramana **80**, 539 (2013) [arXiv:1102.3024 [hep-ph]].

[66] A. Semenov, "*LanHEP - a package for automatic generation of Feynman rules from the Lagrangian. Updated version 3.1*", arXiv:1005.1909 [hep-ph].